The Mechanical Performance of the Fusion Reactor First Wall

Part I:

Steady-state analysis without irradiation effects

W. Daenner

IPP 4/143 October 1976

MAX-PLANCK-INSTITUT FÜR PLASMAPHYSIK

8046 GARCHING BEI MÜNCHEN

MAX-PLANCK-INSTITUT FÜR PLASMAPHYSIK

GARCHING BEI MÜNCHEN

The Mechanical Performance of the Fusion Reactor First Wall

Part I:

Steady-state analysis without irradiation effects

W. Daenner

IPP 4/143 October 1976

Die nachstehende Arbeit wurde im Rahmen des Vertrages zwischen dem Max-Planck-Institut für Plasmaphysik und der Europäischen Atomgemeinschaft über die Zusammenarbeit auf dem Gebiete der Plasmaphysik durchgeführt.

IPP 4/143

The Mechanical Performance of the Fusion Reactor First Wall

Part I: Steady-state analysis without irradiation effects

W. Daenner

October 1976

Abstract

This report describes the steady-state analysis of the mechanical performance of the fusion reactor first wall, excluding any type of irradiation effect. Starting from a nuclear power density profile obtained from neutronics/photonics calculations, we calculate the temperature and stress profiles taking into account external or internal radiation heat sources and mechanical stresses due to pressure loads. The problem is solved for plane, cylindrical and spherical geometries and for different conditions of support. As a final step temperature and stress loads are quoted versus the material's time rupture properties.

The mathematical procedure results in analytical or numerical solutions which have been programmed for the computer. This program has been applied to a number of problems the investigation of which should show justification for some special kinds of simplification usually made. The results show that especially the assumption of a linear variation of the thermal stresses across the wall can lead to erroneous conclusions. The approximation of the real nuclear power density distribution by a constant value results in an underestimation of both the temperature and stress loads, whereas the assumption of radiation being an outside heat source results in an overestimation. Of minor importance is the neglect of Young's modulus, Poisson's ratio, and thermal expansion being temperature dependent. After investigating these simplifications, the influence of the pressure load, choice of geometry and condition of support is studied.

C O N T E N T S

Page

1. INTRODUCTION

The mechanical performance of the first wall poses severe constraints on the design of a fusion reactor which are manifested as a limitation of either the wall loading or the first wall lifetime. Both quantities affect the economics of the reactor very strongly. The wall loading governs inter alia the size of the reactor and a number of its components. The first wall lifetime determines the frequency of first wall replacements and hence, for example, the amount of radioactive waste produced or, together with the length of the shut-down periods, the plant availability. For these reasons, the mechanical performance of the first wall can be considered to be a key problem in fusion reactor engineering.

Up to the present time, very few attempts have been made to get a grasp of this problem [1 - 3]. All these analyses are restricted to distinct geometrical models with fixed dimensions and are imcomplete in one respect or another. In fact, completeness cannot be expected today, because of the very complex nature of an accurate analysis and because of the increasing gap between the amount of information necessary and that available with increasing depth of the analysis. The latter holds especially for the field of neutron radiation damage to the first wall materials.

Although we are fully aware of this situation, fusion reactor systems studies have to deal with this problem in order to give an answer to the question where a certain limit might be and how it depends on the systems parameters involved. To reach this aim the analysis of the mechanical performance of the first wall is intended to proceed step by step. The first step and subject of this report is the steady-state analysis excluding any type of irradiation effects. Inclusion of non-stationary conditions and radiation effects will follow in the future.

The steady-state analysis described here starts by establishing the power density profile. From this the temperature profile is evaluated for a fixed surface temperature at the cool side of the wall. This temperature profile is input to the stress analysis. Here thermal and mechanical stresses in the elastic range are considered. All this is done for a number of basic geometries. To get a first feeling for lifetimes, temperature and stress profile are quoted versus the material's time-rupture properties. This analytical model was programmed for the computer and applied to a series of examples which were selected to show the consequences of the simplifications usually made.

2. THEORETICAL FOUNDATIONS

2.1 Power density profile

Internal heat sources in the wall, which determine the shape of the temperature profile, are due to nuclear reaction processes and the absorption of radiation from the plasma.

As far as nuclear heating is concerned, there are again two separate mechanisms for heat generation. The first is the release of energy to the wall material by neutron reactions with the atoms of the wall, e.g. scattering processes. The second is the absorption of gamma radiation in the wall which is produced either in the wall itself or elsewhere in the blanket, predominantly by (n,γ) reactions. From neutronics and photonics calculations power densities by interval are gained for both the neutron and the gamma contribution. The investigation of a series of such profiles suggests using an equation of the following type for approximating the total nuclear heating q_n :

$$q_n = q_{no} \ (1 - a \cdot x^b). \qquad (1)$$

Here q_{no} [W/cm^3] is the power density at that surface of the wall which is oriented towards the plasma, x [cm] is the

coordinate normal to that surface. In general, q_{no}, a, and b can be gained if at least three points of the profile are known. Therefore, in neutronics/photonics calculations the first wall should be subdivided into at least three intervals.

Fig. 1 shows four typical profiles for a 1 cm thick niobium wall which were calculated in the course of our neutronics/photonics studies. A 200 cm thick blanket of liquid lithium containing different amounts of niobium structure material represented by the equivalent volume fractions ε_s was assumed behind the wall. The absolute values of q_n correspond to a neutron wall loading of 100 W/cm^2. Since the shape of the profile is not changed by applying a different wall loading, a and b can be considered to be characteristics of the blanket type. The surface power density q_{no}, however, varies linearly with the neutron wall loading P_N.

Deviating from this picture, systematic evaluation of stainless steel/liquid lithium blankets [4] shows essentially a linear decrease of the nuclear power density in the wall with x. This case, however, is included in equ. (1) by using b = 1. With a = 0 a constant power density can be simulated. Therefore, equ. (1) is able to characterize a series of interesting nuclear power density profiles.

In addition to the nuclear heating further heating occurs by the absorption of radiation from the plasma. It is assumed in this study that the radiation absorption in the wall and hence the power density q_b follow an exponential decrease

$$q_b = q_{bo} \cdot e^{-\mu x} . \qquad (2)$$

Here, q_{bo} [W/cm^3] again means the power density at that wall surface which is oriented towards the plasma and x [cm] is the coordinate normal to it. The absorption coefficient

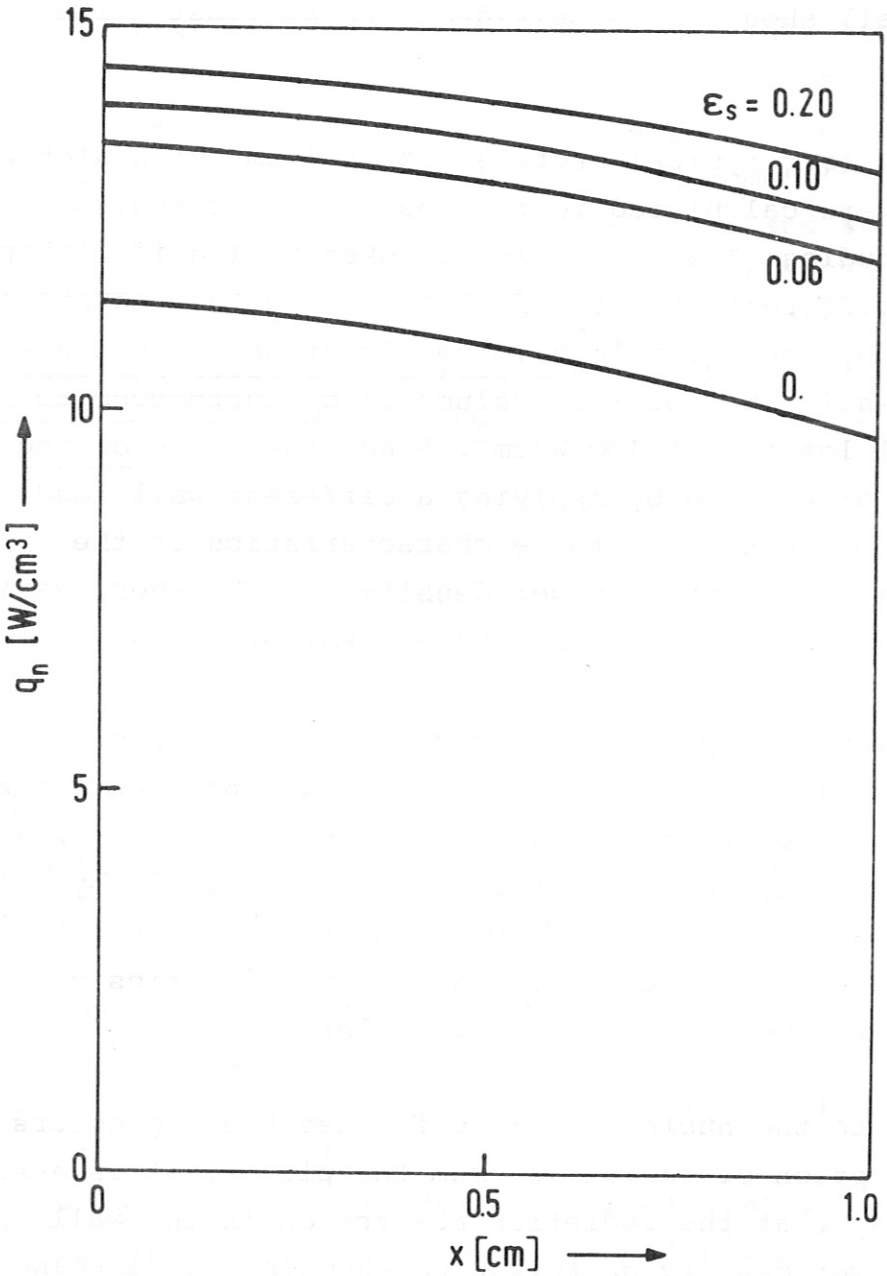

Fig. 1: Profiles of the nuclear power density q_n in a 1 cm niobium first wall for different structure material volume fractions ε_s in a 200 cm liquid lithium blanket. Neutron wall loading is P_N = 100 W/cm^2.

μ [cm^{-1}], which determines the steepness of the power density distribution, is, in principle, a function of the radiation energy. Of the various kinds of radiation emitted by a thermonuclear plasma the bremsstrahlung radiation is the most important, at least under normal operating conditions.

As is discussed in [5], the bremsstrahlung radiation covers a whole energy spectrum the maximum of which varies in size and location with the plasma temperature. For temperatures typical of a D-T fusion reactor (T = 5 ÷ 30 keV) the maximum of the spectrum is located around energies of about 10 - 100 keV. According to [6], in this energy range the predominant absorption mechanism is the photo-effect, characteristic of which are high absorption coefficients μ. For iron, which can be regarded as representative of any type of stainless steel or nickel-base alloy, typical values of μ in this energy range can be found to be between 4 and 80 cm^{-1}. With regard to equ. (2) these figures mean that the radiation power density $q_b(x)$ reaches half the value of q_{bo} at a depth x of about 2 mm in the case μ = 4, and at about 0.1 mm in the case μ = 80. From these figures it can be concluded that it is not necessarily sufficient to treat bremsstrahlung radiation as an external heat source, as is usually done.

An exact treatment of the absorption process would necessitate evaluating an average absorption coefficient $\bar{\mu}$ from the radiation energy spectrum as the first step. This procedure is, however, omitted in this analysis. Instead of this, μ is considered to be a free parameter which can be coupled later to the ion temperature, if necessary.

The absorption coefficient μ is related to a "half--thickness" h,

$$h = \frac{\ell n\ 2}{\mu}\ , \qquad (3)$$

which characterizes the depth at which the radiation power density has decreased to half the value at the surface, q_{bo}.

The surface value, q_{bo}, is calculated from the integral bremsstrahlung wall loading P_B [W/cm^2] by looking at the radiation power per unit length of reactor:

$$2\pi \cdot P_B \cdot r_w = \int_0^{t_{FW}} q_b(x) \cdot 2\pi (r_w + x)\, dx. \qquad (4)$$

Here r_w [cm] means the first wall inner radius and t_{FW} [cm] the first wall thickness. By introducing equ. (2) in equ. (4) and performing the integration we get for q_{bo}

$$q_{bo} = \frac{P_B \cdot r_w \cdot \mu^2}{[(1+\mu r_w) - (1+\mu r_w + \mu t_{FW}) \cdot e^{-\mu t_{FW}}]} \qquad (5)$$

For illustration, in fig. 2 the nuclear and the radiation power density profiles $q_n(x)$ and $q_b(x)$ and the resulting total power density profile $q(x)$ are shown qualitatively. As is suggested in this paper, the total power density can be represented by

$$q(x) = q_n(x) + q_b(x) =$$
$$= q_{no} (1 - a \cdot x^b) + q_{bo} \cdot e^{-\mu x} \qquad (6)$$

2.2 Temperature profile

2.2.1 General way of solving

Having established the power density profile, equ. (6), the next step in the analysis is to evaluate the temperature profile. This is done by solving the differential equation of heat conduction for the steady-state case:

$$\text{div} (\lambda \, \text{grad}\, \vartheta) + q = 0. \qquad (7)$$

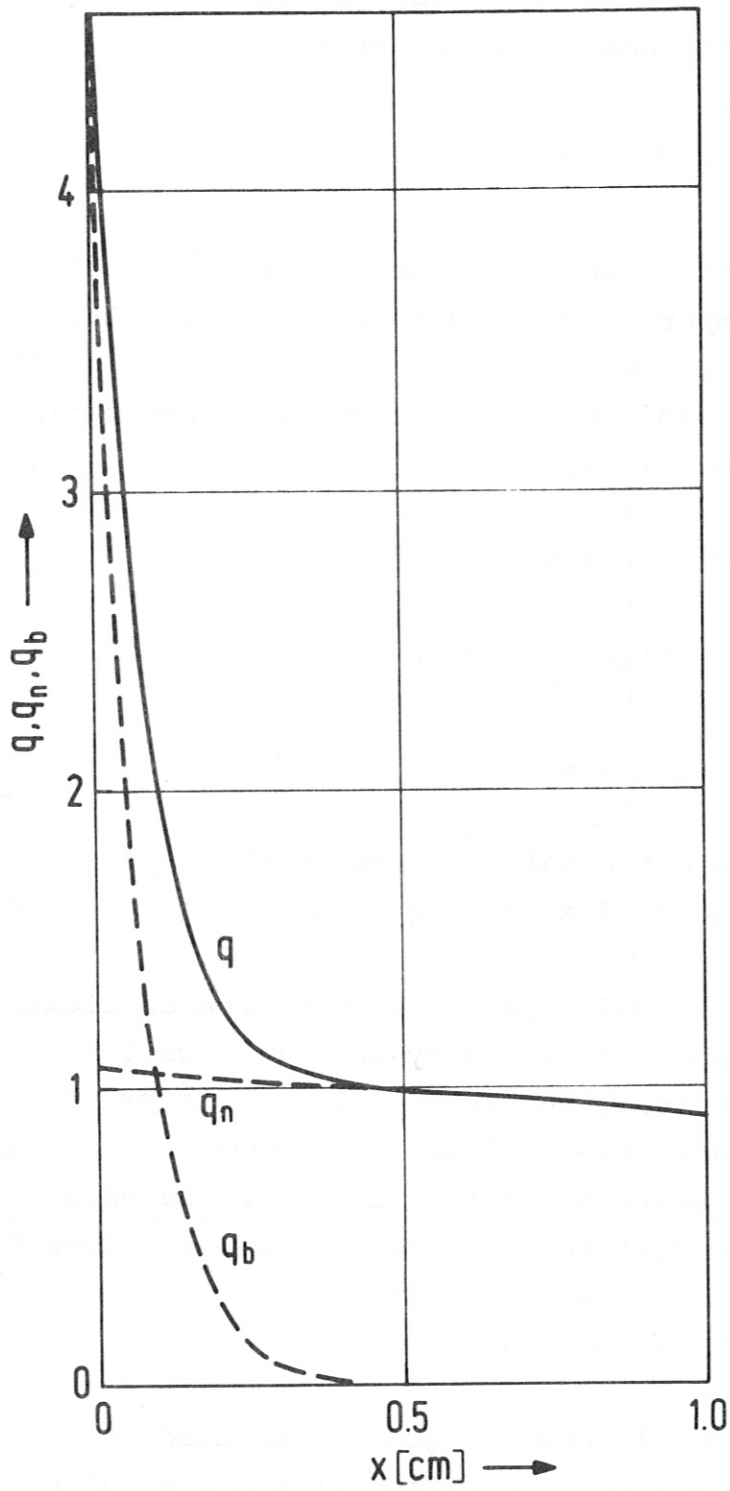

Fig. 2: Profiles of nuclear power density q_n, radiation power density q_b and total power density q in the first wall in arbitrary units.

Here ϑ designates the temperature and λ the thermal conductivity of the wall material. We linearize equ. (7) by introducing the heat flux potential

$$S = \int_{\vartheta_B}^{\vartheta} \lambda(\vartheta')\, d\vartheta' . \qquad (8)$$

In equ. (8) the lower integration limit ϑ_B means any reference temperature, which in all our calculations will be taken as $\vartheta_B = 0\ ^{o}C$. By differentiating equ. (8) with respect to the upper limit of integration and substituting the result in equ. (7) we get

$$\text{div grad } S + q = o \qquad (9)$$

or using the Laplace operator Δ

$$\Delta S + q = o. \qquad (10)$$

To solve this differential equation, the Laplace operator has to be specified according to the geometry used.

Since systems studies need a high degree of flexibility just with respect to geometry, equ. (10) will be solved for plane, cylindrical, and spherical geometries. In the cylindrical and spherical cases an additional distinction will be made between concave and convex curvatures. This total of five different geometrical cases allows considering a variety of possible engineering solutions for the first wall design.

Figs. 3 and fig. 4 show the quantities used in the subsequent analysis for the different geometrical cases, fig. 4 being valid for both cylindrical and spherical geometries. In contrast to the definition of the radii which obviously follows from the design, the definition of the wall depth x is common to all five cases. The origin of this axis is the "hot" surface of the wall which means that surface which is oriented towards the plasma. A further common feature is the use of the

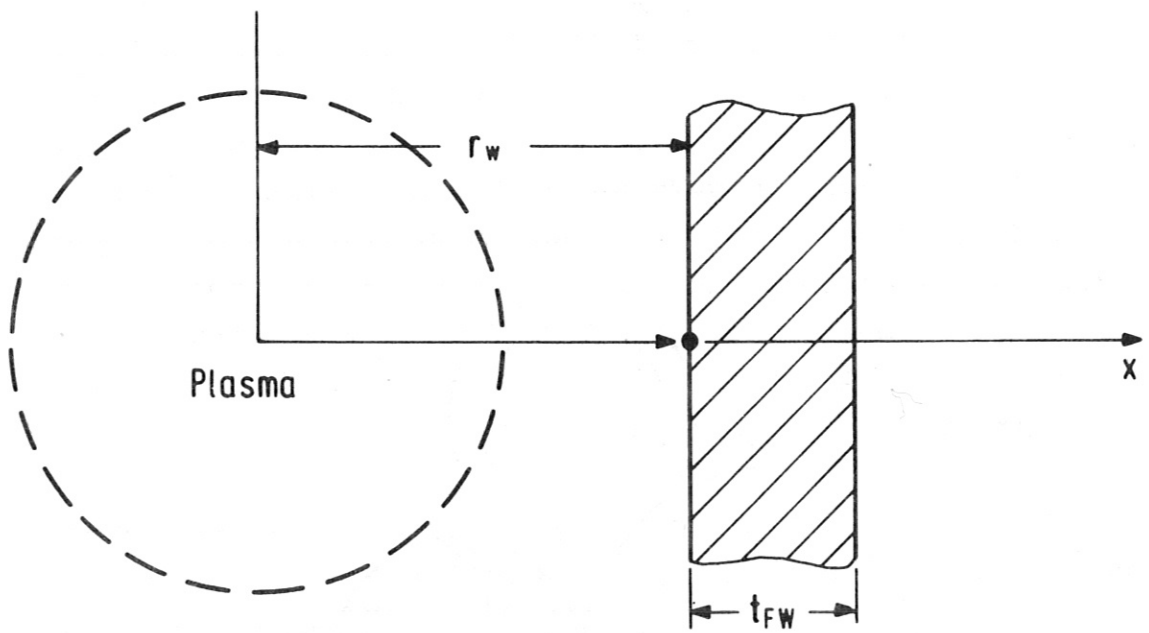

Fig. 3: Definitions for plane geometry.

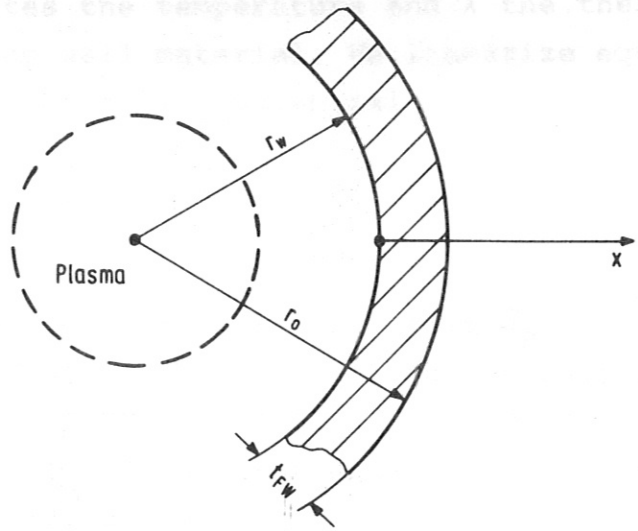

a) concave curvature

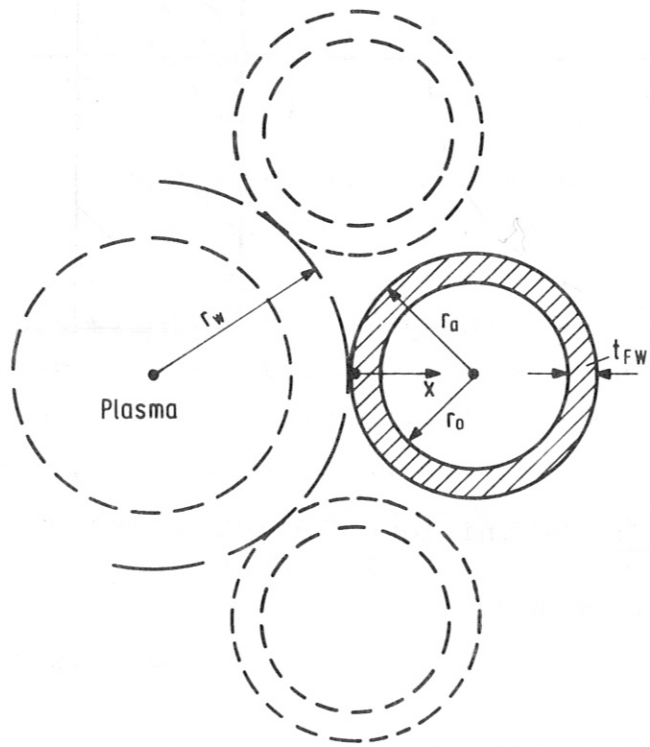

b) convex curvature

Fig. 4: Definitions for cylindrical and spherical geometries.

index "o" for the "cold" surface of the wall. This latter convention is dropped only once: in the case of plane geometry, x at the cold surface is called t_{FW} which is the first wall thickness.

Before entering the procedure of solving equ. (10) one assumption common to all five cases shall be explained. In all evaluations it is assumed that the power density profile only depends on the wall depth x and not on the radius r. This assumption should prove to be sufficient for the case of concave shells. It is a simplification in the cases of convex shells especially when larger ratios t_{FW}/r_o are considered. For this type of geometry, however, a second simplification is implicitly involved which may be more significant than that just described. This simplification is the neglect of circumferential and axial variations which could only be treated by applying two or even three-dimensional methods. This, however, is beyond the scope of this first part of the report.

By specifying the Laplace operator equ. (10) reads as follows for the plane (case a), cylindrical (case b), and spherical (case c) geometries:

$$\text{a)} \quad \frac{d^2S}{dr^2} + q(r) = 0, \tag{11a}$$

$$\text{b)} \quad \frac{d^2S}{dr^2} + \frac{1}{r}\frac{dS}{dr} + q(r) = 0, \tag{11b}$$

$$\text{c)} \quad \frac{d^2S}{dr^2} + \frac{2}{r}\frac{dS}{dr} + q(r) = 0. \tag{11c}$$

(To be systematic, we write r in place of x for the plane geometry case.)
These equations are usually solved by substituting

$$\frac{dS}{dr} = \frac{1}{r^n} \cdot y. \tag{12}$$

Here the exponent n is the quantity which discriminates the three types of geometry:

$$\begin{aligned} n &= 0 \quad \text{plane geometry,} \\ n &= 1 \quad \text{cylindrical geometry,} \\ n &= 2 \quad \text{spherical geometry.} \end{aligned} \tag{13}$$

Introducing equ. (12) into equs. (11) yields

$$\frac{dy}{dr} = -r^n \, q(r). \tag{14}$$

In this way equs. (11) are solved by integrating equ. (14) and equ. (12) twice. The first integration of equ. (14) yields:

$$y = -\int_{r_1}^{r} r'^n \, q(r') \, dr' + C_1. \tag{15}$$

For simplification we abbreviate

$$Q_n(r_1,r) = \int_{r_1}^{r} r'^n \, q(r') \, dr'. \tag{16}$$

The arguments r_1 and r of the function Q_n denote the lower and upper integration limits respectively. Equ. (15) now reads

$$y = - Q_n(r_1 r) + C_1. \tag{17}$$

For the determination of the integration constant C_1 we use the boundary condition which says that at the "cool" side of the wall the temperature gradient is determined by the total heat flux density Q at this position:

$$-\lambda(\vartheta) \cdot \left(\frac{d\vartheta}{dr}\right)_{r = r_o} = Q. \tag{18}$$

Equ. (18) is also valid for the plane geometry case, where, as indicated above, r has to be replaced by x and r_o by t_{FW}. If we consider the left hand-side of equ. (18) we find the following relations from equs. (8) and (12):

$$-\lambda(\vartheta)\left(\frac{d\vartheta}{dr}\right)_{r=r_o} = -\left(\frac{ds}{dr}\right)_{r=r_o} = -\frac{(y)_{r=r_o}}{r_o^{\,n}} \,. \tag{19}$$

To find the total heat flux density Q at the "cool" side of the wall, an integration over the power density profile is necessary. This total power has to pass through the wall surface defined by r_o. Although the power density profile q(r) already contains a contribution which is due to radiation heating we assume here that there may be an additional heat source outside the wall producing an additional heat flux density P_R [W/cm^2]. Taking all this into account, we arrive at the following expression for Q:

$$Q = \frac{1}{r_o^{\,n}} \int_{r_1}^{r_o} (r')^n \cdot q(r')\, dr' + P_R \cdot \frac{r_1^{\,n}}{r_o^{\,n}} \,. \tag{20}$$

The introduction of P_R provides the possibility of taking any other heat sources outside the wall into account, or of treating bremsstrahlung radiation as an external source for comparison. For this case one has to set $P_R = P_B$ and $q_{bo} = 0$.

Equ. (16) shows that equ. (20) can also be written as

$$Q = \frac{1}{r_o^{\,n}} \cdot Q_n\,(r_1, r_o) + P_R \cdot \left(\frac{r_1}{r_o}\right)^n \,. \tag{21}$$

With equ. (21) and the third term of equ. (19) the boundary condition, equ. (18), becomes

$$-\frac{(y)_{r=r_o}}{r_o^{\,n}} = \frac{1}{r_o^{\,n}} \cdot Q_n\,(r_1, r_o) + P_R \cdot \left(\frac{r_1}{r_o}\right)^n \tag{22}$$

The left-hand side of equ. (22) can be expressed by introducing the result of the first integration in the form of equ. (17), yielding

$$- \frac{1}{r_o^n} [- Q_n(r_1,r_o) + C_1] = \frac{1}{r_o^n} \cdot Q_n(r_1,r_o) + P_R \cdot \frac{r_1^n}{r_o^n}. \qquad (23)$$

This equ. yields the integration constant C_1:

$$C_1 = - P_R \cdot r_1^n. \qquad (24)$$

The final result of the first integration, equ. (17), can be written as

$$y = - Q_n(r_1,r) - P_R \cdot r_1^n. \qquad (25)$$

This solution has to be introduced into equ. (12), and this equation has to be integrated to yield S as a function of r:

$$S = -\int_{r_1}^{r} \frac{1}{(r')^n} [Q_n(r_1,r') + P_R \cdot r_1^n] \, dr' + C_2. \qquad (26)$$

Just as in the case of the first integration we introduce for simplification the abbreviation

$$Y_n(r_1,r) = \int_{r_1}^{r} \frac{1}{(r')^n} [Q_n(r_1,r') + P_R \cdot r_1^n] \, dr', \qquad (27)$$

the arguments of this function again denoting the integration limits. Equ. (26) now reads

$$S = - Y_n(r_1,r) + C_2. \qquad (28)$$

To obtain C_2, a second boundary condition must be met. For this purpose the temperature at the "cool" side of the wall is fixed at ϑ_o. Due to equ. (8) this temperature corresponds to a heat flux potential S_o:

$$S_o = \int_{\vartheta_B}^{\vartheta_o} \lambda(\vartheta') \, d\vartheta'. \qquad (29)$$

By introducing S_o at the location $r = r_o$ into equ. (28) the integration constant C_2 follows directly:

$$C_2 = S_o + Y_n(r_1, r_o) \tag{30}$$

and for the solution, equ. (28), we get

$$S = S_o + Y_n(r_1, r_o) - Y_n(r_1, r). \tag{31}$$

Since the second and the third terms of the right-hand side of this equation mean the difference of two integrals with different integration limits but the same integrand, we can write equ. (31) using the notation defined above:

$$S = S_o + Y_n(r, r_o). \tag{32}$$

This equation is the solution of the problem because the temperature profile $\vartheta(r)$ can be directly assigned to the profile $S(r)$ by inverting equ. (8).

2.2.2 Specialization to real geometries

The preceding section was devoted to the general solution of the problem of evaluating the temperature profile $\vartheta(r)$ in the first wall from a power density profile $q(r)$. The temperature profile $\vartheta(r)$ can easily be derived from that of the heat flux potential $S(r)$. This latter profile was found to be

$$S(r) = S_o + Y_n(r, r_o) \tag{33}$$

with the abbreviations

$$Y_n(r, r_o) = \int_r^{r_o} \frac{1}{(r')^n} \left[Q_n(r_1, r') + P_R \cdot r_1^n \right] dr', \tag{34}$$

$$Q_n(r_1, r) = \int_{r_1}^{r} (r')^n \, q(r') \, dr', \tag{35}$$

and the power density profile

$$q(r) = q_{no} \ (1 - a.x^b) + q_{bo} \cdot e^{-\mu x}. \qquad (36)$$

The specialization of these equations to the five different types of geometrical arrangements (plane, cylindrical concave, cylindrical convex, spherical concave, spherical convex) is done by choosing the appropriate quantities for n, r, r_o, and r_1 according to figs. (3) and (4) and equ. (13) respectively.

For convenience, the definition of these quantities is summarized in table I.

Table I: Specialized parameters for the different geometrical arrangements

Type of geometry	n	r	r_o	r_1
plane	0	x	t_{FW}	0
cylindrical concave	1	$r_w + x$	r_o	r_w
cylindrical convex	1	$r_a - x$	r_o	r_a
spherical concave	2	$r_w + x$	r_o	r_w
spherical convex	2	$r_a - x$	r_o	r_a

2.2.2.1 Plane geometry

For the case of plane geometry the power density profile is given by the original equation, equ. (36):

$$q(x) = q_{no} \ (1 - a \ x^b) + q_{bo} \cdot e^{-\mu x}. \qquad (37)$$

The specialization of equ. (35) to plane geometry using the notation of table I yields

$$Q_o(0,x) = \int_0^x q(x) \ dx. \qquad (38)$$

Introducting q(x) from equ. (37) and performing the integration results in

$$Q_o(0,x) = q_{no}\ (x - \frac{a}{b+1} \cdot x^{b+1}) + \frac{q_{bo}}{\mu}\ (1 - e^{-\mu x}). \tag{39}$$

Similarly equ. (34) can be specialized yielding

$$Y_o(x,t_{FW}) = \int_x^{t_{FW}} [Q_o(0,x') + P_R]\ dx'. \tag{40}$$

By inserting equ. (39) into equ. (40) and performing the integration, we get

$$Y_o(x,t_{FW}) = q_{no} \left[\frac{t_{FW}^2 - x^2}{2} - \frac{a}{(b+1)\cdot(b+2)}\ (t_{FW}^{b+2} - x^{b+2}) \right] +$$

$$+ \frac{q_{bo}}{\mu 2}\ (e^{-\mu t_{FW}} - e^{-\mu x}) + (\frac{q_{bo}}{\mu} + P_R)\ (t_{FW} - x). \tag{41}$$

By using this equation $\vartheta(x)$ can be obtained from

$$S(x) = S_o + Y_o(x,\ t_{FW}). \tag{42}$$

2.2.2.2 _ Cylindrical geometry, concave curvature

In accordance with table I we substitute

$$r = r_w + x. \tag{43}$$

Because of the assumption that the power density only depends on the wall depth x it follows that

$$q(r) = q(r_w + x) = q_{no}\ (1 - a\ x^b) + q_{bo} \cdot e^{-\mu x}. \tag{44}$$

The evaluation of equ. (35) specialized to the type of geometry discussed here,

$$Q_1(r_w,r) = \int_{r_w}^{r} r'q(r')\ dr' \tag{45}$$

can therefore be done by an integration with respect to x:

$$Q_1(r_w,r) = \int_o^x (r_w + x') \cdot q(r_w + x'), dx'. \qquad (46)$$

If the right-hand side of equ. (44) is introduced in equ. (46) it becomes obvious that

$$Q_1(r_w,r) = r_w \cdot Q_o(0,x) + Q_{11}(0,x), \qquad (47)$$

$Q_o(0,x)$ being just the equivalent solution of the plane problem, equ. (39), and $Q_{11}(0,x)$ defined by

$$Q_{11}(0,x) = \int_o^x x'q(x') \, dx' , \qquad (48)$$

the solution of which is

$$Q_{11}(0,x) = q_{no}\left[\frac{x^2}{2} - \frac{a}{b+2} x^{b+2}\right] + \frac{q_{bo}}{\mu^2} [1 - (1+\mu x) e^{-\mu x}] . \qquad (49)$$

To evaluate equ. (34), which, in specialized form, reads

$$Y_1(r,r_o) = \int_r^{r_o} \frac{1}{r^2} [Q_1(r_w,r') + P_R r_w] \, dr' \qquad (50)$$

we may resubstitute $(r - r_w)$ for x in equ. (47) and accordingly in equ. (39) and equ. (49). Then we would have to replace Q_1 in equ. (50) by these expressions, divide each term by r and integrate each new term with respect to r. A term by term examination shows that this would involve integrals of the type $\int \frac{e^{-\mu x}}{x^n} dx$, generally known as the exponential integral, which can only be analytically solved by a series expansions. An attempt to do this with realistic values for μ and x shows a very poor convergence behaviour of this series. Therefore, it was decided to solve equ. (50) numerically. The results of this numerical integration are then utilized to calculate S(r) from equ. (33).

2.2.2.3 Cylindrical geometry, convex curvature

In contrast to the concave curvature in this case we have to use another substitution

$$r = r_a - x, \qquad (51)$$

which yields the power density as

$$q(r) = q(r_a - x) = q_{no}\ (1 - a.x^b) + q_{bo} \cdot e^{-\mu x}. \qquad (52)$$

As in the previous case we obtain the specialized equ. (35) by replacing r_1 by r_a instead of r_w:

$$Q_1(r_a,r) = \int_{r_a}^{r} r'q(r')\ dr'. \qquad (53)$$

By utilizing again the above substitution equ. (53) reads

$$Q_1(r_a,r) = \int_{o}^{x} (r_a-x') \cdot q(r_a-x')\ dx', \qquad (54)$$

the solution of which is equivalent to equ. (46):

$$Q_1\ (r_a,r) = r_a \cdot Q_o(o,x) - Q_{11}(o,x). \qquad (55)$$

Equ. (55) now has to be introduced in the specialized equ. (34):

$$Y_1(r,r_o) = \int_{r}^{r_o} \frac{1}{r'}\ [Q_1(r_a,r') + P_R \cdot r_a]\ dr', \qquad (56)$$

which again has to be solved numerically to yield S(r) and and ϑ(r) as the final results.

2.2.2.4 Spherical geometry, concave curvature

In accordance with table I we use the same substitution as for the cylindrical geometry in the case of concave curvature, expressed by equ. (43). Thus, the power density agrees completely with equ. (44):

$$q(r) = q(r_w + x) = q_{no}\ (1- a.x^b) + q_{bo}\ e^{-\mu x}. \qquad (57)$$

The specialization of equ. (35), however, now yields

$$Q_2(r_w,r) = \int_{r_w}^{r} (r')^2\ q(r')\ dr'. \qquad (58)$$

Introducing the substitution for r into this equation results in

$$Q_2(r_w,r) = \int_0^x [r_w^2 + (x')^2 + 2r_w x'] \cdot q(r_w + x')\, dx'. \quad (59)$$

Again,we can split up this integral to utilize, at least partly, solutions which are already known:

$$Q_2(r_w,r) = r_w^2 \cdot Q_o(0,x) + 2r_w \cdot Q_{11}(0,x) + Q_{22}(0,x) \quad (60)$$

Here only the last term has yet to be specified:

$$Q_{22}(0,x) = \int_0^x (x')^2\, q(x')\, dx' \quad (61)$$

The solution of this integral is

$$Q_{22}(0,x) = \frac{q_{no}}{3} x^3 - \frac{q_{no} \cdot a}{b+3} \cdot x^{b+3} +$$

$$+ \frac{q_{bo}}{\mu} \left\{ \frac{2}{\mu^2} - \left[x^2 + \frac{2x}{\mu} + \frac{2}{\mu^2}\right] \cdot e^{-\mu x} \right\}. \quad (62)$$

Represented by its single terms according to equs.(39), (49), and (62), equ. (60) finally has to be introduced in the specialized form of equ. (34):

$$Y_2(r,r_o) = \int_r^{r_o} \frac{1}{(r')^2} [Q_2(r_w,r') + P_R \cdot r_w^2]\, dr'. \quad (63)$$

For the same reasons as explained in connection with equ. (50),this equation can only be solved numerically, too. The remaining procedure corresponds exactly to those of the former cases.

2.2.2.5 Spherical geometry, convex curvature

As in the corresponding case for the cylindrical geometry the power density profile is represented there by

$$q(r) = q(r_a - x) = q_{no} (1 - a \cdot x^b) + q_{bo} \cdot e^{-\mu x} \quad (64)$$

again utilizing the substitution defined by equ. (51).

The specialized equ. (35) becomes

$$Q_2(r_a,r) = \int_{r_a}^{r} (r')^2 \, q(r') \, dr'. \qquad (65)$$

Introducing the substitution into this equation yields

$$Q_2(r_a,r) = \int_{0}^{x} [r_a^2 + (x')^2 - 2r_a x'] \cdot q(r_a - x') \, dx'. \qquad (66)$$

By splitting up the integral we obtain

$$Q_2(r_a,r) = r_a^2 \cdot Q_0(0,x) - 2r_a \, Q_{11}(0,x) + Q_{22}(0,x). \qquad (67)$$

Again, $Q_{22}(0,x)$ is defined by equ. (61) or equ. (62).
Equ. (67) has to be inserted in the specialized equ. (34):

$$Y_2(r,r_o) = \int_{r}^{r_o} \frac{1}{(r')^2} [Q_2(r_a,r') + P_R \cdot r_a^2] \, dr' \qquad (68)$$

to yield finally S(r) and from this profile the temperature profile $\vartheta(r)$.

2.3 Stress profile

In most fusion reactor design studies the stress analysis of the first wall is treated very roughly. This may be due to the fact that a complete analysis is rather complex, and that it requires a lot of information which is not yet available for fusion reactor conditions. The latter holds especially for the field of irradiation effects, which have to be taken into account in such an analysis.

As was indicated in the introduction, we do not intend to achieve the aim of a complete model at once. We start here with the solution of the steady-state problem in the

elastic domain and do not care about irradiation effects. Subsequent parts of this report shall summarize the results of the analysis where these restrictions will be removed step by step. The problem treated here will be exclusively concerned with mechanical and thermal stresses. The solution of this problem can, in principle, be found in the literature [7 - 9].In spite of this fact, some of the main ideas and steps of the analysis shall be repeated here because they are a guide for the treatment of the more complicated problems to come.

In the following subsections we are essentially following the presentation of Timoshenko and Goodier [7]. We start with the treatment of the cylindrical geometry followed by the spherical and plane geometries. Finally, some remarks about the toroid are made.

2.3.1 Cylindrical geometry

The analysis generally starts with the statement that the three components of strain can be expressed as the sum of two contributions:

$$\varepsilon_j = \varepsilon_j^{(E)} + \varepsilon^{(T)} \tag{69}$$

Here j denotes, for the case of cylindrical geometry, the radial, azimuthal, and axial components, respectively ($j = r, \theta, z$); $\varepsilon_j^{(E)}$ are the three components of elastic strain; $\varepsilon^{(T)}$ is the thermal expansion strain, which is assumed to be isotropic.

The elastic strains are given by Hooke's law:

$$\varepsilon_r^{(E)} = \frac{1}{E} [\sigma_r - \nu(\sigma_\theta + \sigma_z)] , \tag{70}$$

$$\varepsilon_\theta^{(E)} = \frac{1}{E} [\sigma_\theta - \nu(\sigma_r + \sigma_z)] , \tag{71}$$

$$\varepsilon_z^{(E)} = \frac{1}{E} [\sigma_z - \nu(\sigma_r + \sigma_\theta)] , \tag{72}$$

the thermal expansion strain by

$$\varepsilon^{(T)} = \alpha \Delta \vartheta. \tag{73}$$

In these equations σ_r, σ_θ, and σ_z are the radial, azimuthal, and axial stresses, respectively, E is Young's modulus, and $\Delta\vartheta$ stands for a temperature difference

$$\Delta\vartheta = \vartheta - \vartheta^{(0)}, \tag{74}$$

where $\vartheta^{(0)}$ is defined as that temperature at which no thermal stresses occur. The coefficient α in equ. (73) is to be interpreted as the average thermal expansion coefficient in the temperature interval between $\vartheta^{(0)}$ and ϑ. It is defined by

$$\alpha = \frac{\int_{\vartheta^{(0)}}^{\vartheta} \alpha(\vartheta')\, d\vartheta'}{\vartheta - \vartheta^{(0)}}. \tag{75}$$

2.3.1.1 Zero expansion in axial direction

The first case generally considered is that in which an axial expansion of the cylinder is completely suppressed (see Fig. 5a). This means that

$$\varepsilon_z = \varepsilon_z^{(E)} + \varepsilon^{(T)} = 0. \tag{76}$$

Introducing equ. (72) and equ. (73) into this condition the axial stress component can be evaluated to be

$$\sigma_z = \nu(\sigma_r + \sigma_\theta) - \alpha E \Delta\vartheta. \tag{77}$$

When equ. (69) is written for the two remaining components, σ_z can be eliminated by inserting equ. (77). This results in

$$\varepsilon_r - (1+\nu)\alpha\nu\vartheta = \frac{1-\nu^2}{E}\left(\sigma_r - \frac{\nu}{1-\nu}\sigma_\theta\right), \tag{78}$$

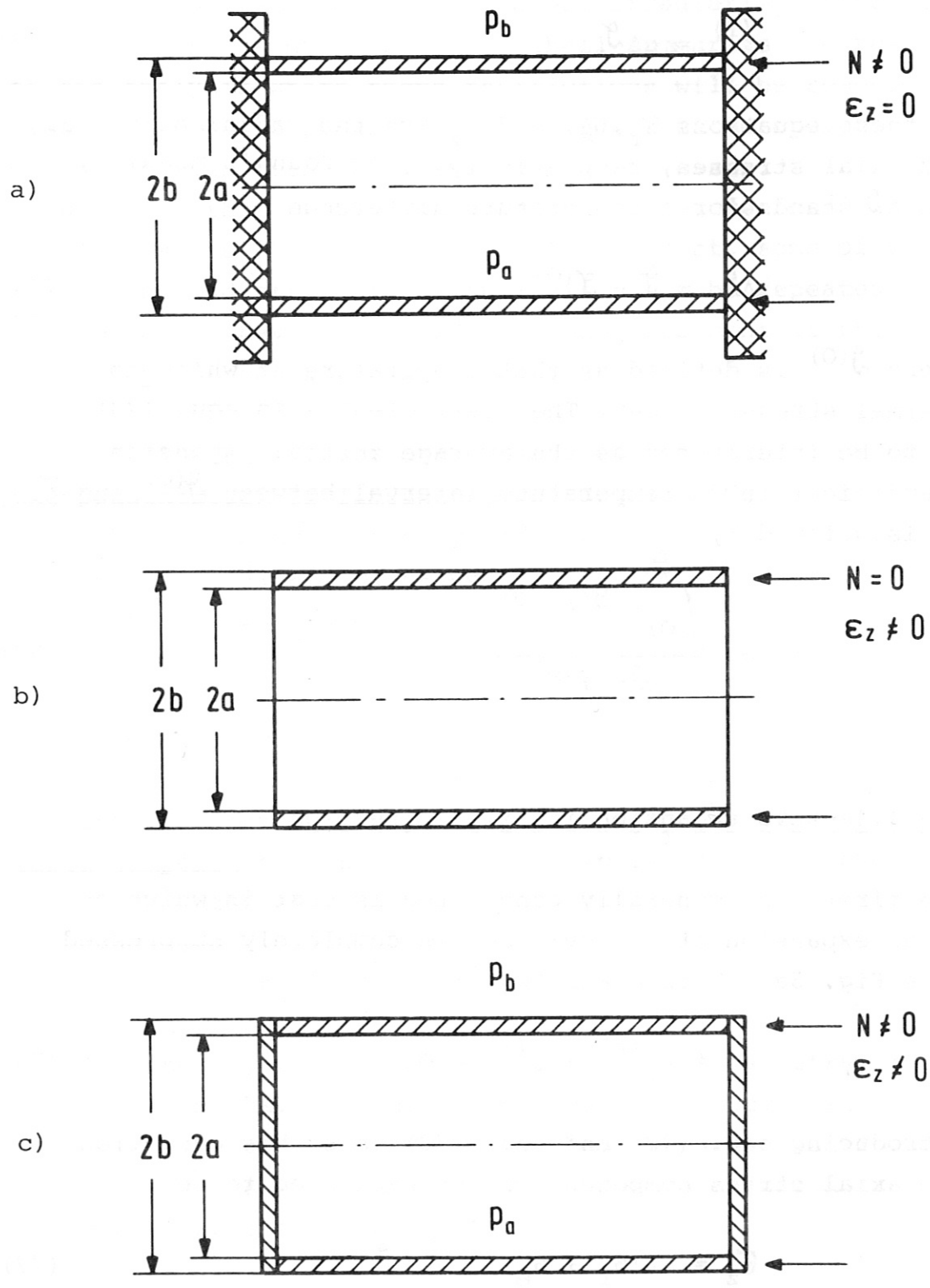

Fig. 5: The different cases for cylindrical stress analysis

$$\varepsilon_\theta - (1+\nu)\alpha\Delta\vartheta = \frac{1-\nu^2}{E}\left(\sigma_\theta - \frac{\nu}{1-\nu}\sigma_r\right). \tag{79}$$

By solving equ. (78) and equ. (79) for the stress components it is found that

$$\sigma_r = \frac{E\ (1-\nu)}{(1+\nu)\ (1-2\nu)}\left[\varepsilon_r + \frac{\nu}{1-\nu}\varepsilon_\theta - \frac{1+\nu}{1-\nu}\alpha\Delta\vartheta\right]. \tag{80}$$

$$\sigma_\theta = \frac{E\ (1-\nu)}{(1+\nu)\ (1-2\nu)}\left[\varepsilon_\theta + \frac{\nu}{1-\nu}\varepsilon_r - \frac{1+\nu}{1-\nu}\alpha\Delta\vartheta\right]. \tag{81}$$

In the cylindrical geometry the stresses σ_r and σ_θ have to obey the equation of equilibrium:

$$\frac{d\sigma_r}{dr} + \frac{\sigma_r - \sigma_\theta}{r} = 0. \tag{82}$$

By substituting σ_r and σ_θ from equ. (80) and equ. (81) we get from equ. (82)

$$r\frac{d\varepsilon_r}{dr} + \frac{\nu}{1-\nu}\,r\frac{d\varepsilon_\theta}{dr} + \frac{1-2\nu}{1-\nu}(\varepsilon_r - \varepsilon_\theta) = \frac{1+\nu}{1-\nu}\cdot\alpha\cdot r\ \frac{d\Delta\vartheta}{dr}. \tag{83}$$

The compatibility of strains requires

$$\varepsilon_r = \frac{du}{dr}, \tag{84}$$

$$\varepsilon_\theta = \frac{u}{r}, \tag{85}$$

where u is the radial displacement. With the derivatives of ε_r and ε_θ

$$\frac{d\varepsilon_r}{dr} = \frac{d^2u}{dr^2}, \tag{86}$$

$$\frac{d\varepsilon_\theta}{dr} = \frac{1}{r}\frac{du}{dr} - \frac{u}{r^2}, \tag{87}$$

and equs. (84) and (85) we obtain from equ. (83) a differential equation for the radial displacement u which reads

$$\frac{d^2u}{dr^2} + \frac{1}{r}\frac{du}{dr} - \frac{u}{r^2} = \frac{1+\nu}{1-\nu}\cdot\alpha\cdot\frac{d\Delta\vartheta}{dr}. \tag{88}$$

The solution of this equation is

$$u = \frac{1+\nu}{1-\nu} \cdot \alpha \cdot \frac{1}{r} \int r' \Delta \vartheta(r') dr' + C_1 \cdot r + \frac{C_2}{r} . \qquad (89)$$

When this solution is introduced into equs. (84) and (85) we obtain the strains:

$$\varepsilon_r = \frac{1+\nu}{1-\nu} \cdot \alpha \left[\Delta \vartheta(r) - \frac{1}{r^2} \int r' \Delta \vartheta(r') dr' \right] + C_1 - \frac{C_2}{r^2}, \qquad (90)$$

$$\varepsilon_\Theta = \frac{1+\nu}{1-\nu} \cdot \alpha \cdot \frac{1}{r^2} \int r' \Delta \vartheta(r') dr' + C_1 + \frac{C_2}{r^2} . \qquad (91)$$

These solutions introduced in equs. (80) and (81) yield the stresses

$$\sigma_r = \frac{E}{(1+\nu)(1-2\nu)} \cdot C_1 - \frac{E}{1+\nu} \cdot \frac{C_2}{r^2} - \frac{E}{1-\nu} \cdot \alpha \frac{1}{r^2} \int r' \Delta \vartheta(r') dr', \qquad (92)$$

$$\sigma_\Theta = \frac{E}{(1+\nu)(1-2\nu)} \cdot C_1 + \frac{E}{1+\nu} \cdot \frac{C_2}{r^2} + \frac{E\alpha}{1-\nu} \cdot \frac{1}{r^2} \int r' \Delta \vartheta(r') dr' - \frac{E\alpha}{1-\nu} \Delta \vartheta(r). \qquad (93)$$

In order to determine the integration constants C_1 and C_2, we have to apply boundary conditions. With regard to a possible generalization of the problem we apply the procedure to a hollow cylinder with inner radius a and outer radius b and we request the radial stresses σ_r at the surfaces to be equal to equivalent pressure loads p_a and p_b respectively. From this it follows that

$$\sigma_r \ (r=a) = - p_a, \qquad (94)$$

$$\sigma_r \ (r=b) = - p_b. \qquad (95)$$

From these conditions the constants C_1 and C_2 are found to be

$$C_1 = \frac{(1+\nu)(1-2\nu)}{E} \left[\frac{b^2}{b^2-a^2} (p_a - p_b) - p_a \right] +$$

$$+ \frac{(1+\nu)(1-2\nu)}{(1-\nu)} \cdot \frac{1}{b^2-a^2} \cdot \alpha \int_a^b r' \Delta \vartheta(r') dr', \qquad (96)$$

$$C_2 = \frac{(1+\nu)}{E} \cdot \frac{a^2 b^2}{b^2-a^2}(p_a-p_b) +$$

$$+ \frac{1+\nu}{1-\nu} \frac{a^2}{b^2-a^2} \alpha \int_a^b r' \Delta \vartheta(r') dr'. \qquad (97)$$

By introducing C_1 and C_2 from equs. (96) and (97) into equs. (92) and (93) the final solutions for the radial and azimuthal stresses are obtained:

$$\sigma_r = - p_a + (p_a-p_b) \cdot \frac{b^2}{b^2-a^2}\left(1 - \frac{a^2}{r^2}\right) +$$

$$+ \frac{E\alpha}{1-\nu}\left[\frac{r^2-a^2}{b^2-a^2} \cdot \frac{1}{r^2}\int_a^b r' \Delta\vartheta(r') dr' - \frac{1}{r^2}\int_a^r r' \Delta\vartheta(r') dr'\right], \qquad (98)$$

$$\sigma_\theta = - p_a + (p_a-p_b) \frac{b^2}{b^2-a^2}\left(1 + \frac{a^2}{r^2}\right) +$$

$$+ \frac{E\alpha}{1-\nu}\left[\frac{r^2+a^2}{b^2-a^2} \cdot \frac{1}{r^2}\int_a^b r' \Delta\vartheta(r') dr' + \frac{1}{r^2}\int_a^r r' \Delta\vartheta(r') dr' - \Delta\vartheta(r)\right]. \qquad (99)$$

To obtain the axial stress, σ_z, we have to evaluate equ. (77) by inserting equ. (98) and equ. (99). Doing this we arrive at

$$\sigma_z = 2\nu \left[- p_a + (p_a-p_b) \frac{b^2}{b^2-a^2}\right] +$$

$$+ \frac{E\alpha}{1-\nu}\left[\frac{2\nu}{b^2-a^2}\int_a^b r' \Delta\vartheta(r') dr' - \Delta\vartheta(r)\right] \qquad (100)$$

as the final solution for the axial stress in the case that free axial expansion of the cylinder is completely suppressed.

Normal forces occur at the end planes of the cylinder which can be calculated from σ_z. These normal forces are a necessary consequence of the assumption of a zero axial expansion.

During the derivation of these equations we deviated from Timoshenko's procedure only in one point. With equs. (94) and (95) we chose different boundary values for the radial stress σ_r. While Timoshenko assumed a zero pressure load we decided, with regard to the first wall problem in a fusion reactor, to account for the possibility of having a certain pressure either inside or outside the cylinder. In comparing Timoshenko's results with those presented here we see that the three stress components σ_j are represented by

$$\sigma_j = \sigma_j^{(M)} + \sigma_j^{(T)}, \tag{101}$$

$\sigma_j^{(M)}$ being the contribution resulting from the mechanical load, $\sigma_j^{(T)}$ being that resulting from the thermal load.

2.3.1.2 Free expansion in axial direction

In contrast to the case just treated, it shall now be assumed that the cylinder can undergo free expansion in the axial direction. A solution of this case restricted, however, to thermal stresses only has been presented by Timoshenko [7]. Since no internal or external pressures are applied in this case, the problem can be considered to be equivalent to Fig. 5b, which shows a hollow cylinder completely open at both end planes.

According to Timoshenko, there is no need to repeat the entire procedure once more on the assumption that equ. (76) does not hold. He states - without proof - that equ. (98) and equ. (99), which describe the radial and the azimuthal stress distributions, remain unchanged, and that it is possible to derive the axial stress component σ_z from a consideration of axial forces only.

In the case where the cylinder was prevented from free expansion a normal force at the end planes occurred owing

to the axial stresses σ_z. With a completely unrestrained hollow cylinder such a normal force may, however, not occur. This condition can formally be met by superposing a uniformly distributed axial stress K_z which just equilibrates the stress distribution defined by equ. (100):

$$K_z \cdot \pi(b^2-a^2) = -\int_a^b 2\pi r' \sigma_z(r')dr'. \tag{102}$$

The new axial stress distribution $\bar{\sigma}_z$ for this case is then given by

$$\bar{\sigma}_z = \sigma_z + K_z, \tag{103}$$

the result being

$$\bar{\sigma}_z = \frac{E\alpha}{1-\nu}\left[\frac{2}{b^2-a^2}\int_a^b r'\Delta\vartheta(r')dr' - \Delta\vartheta(r)\right]. \tag{104}$$

This expression for $\bar{\sigma}_z$ is obtained independently of the assumption whether there is an additional pressure load p_a and/or p_b or not. Just for physical reasons the contribution of $\sigma_z^{(M)}$ to the total σ_z has to vanish because we are considering an open cylinder. The axial stress is exclusively due to thermal effects.

The real and practical case for fusion reactor blanket application will most probably be defined as one in between these two extrema. It will be, as shown in fig. 5c, an axially closed cylinder, but having the possibility of free axial expansion. In spite of the free expansion there will be a normal force at the end planes because of an either internal or external pressure load. The equivalent axial stress K_z has to be added to the axial stress $\bar{\sigma}_z$ valid for the free expanding cylinder, yielding the total axial stress $\bar{\bar{\sigma}}_z$ for this case:

$$\bar{\bar{\sigma}}_z = \bar{\sigma}_z + \bar{K}_z = \sigma_z + K_z + \bar{K}_z. \tag{105}$$

For the case of internal pressure, p_a, $\bar{K}_z$ is defined by

$$\bar{K}_z = \frac{a^2}{b^2-a^2} \cdot p_a. \tag{106}$$

For the case of external pressure, p_b, $\bar{K}_z$ additionally depends on the geometry outside the cylinder considered. Here we restrict ourselves to the arrangement of two concentric cylinders, as shown in fig. 6. With respect to the inner cylinder p_b works as an external pressure. The resulting axial stress $\bar{K}_z$ in the inner cylinder becomes

$$\bar{K}_z = - \frac{c^2-b^2}{(b^2-a^2)} \cdot \frac{(c+d) - \sqrt{2\ (c^2+b^2)}}{(c+d) - (a+b)} \cdot p_b \tag{107}$$

While the meaning of a and b is the same as before, c and d are the inner and outer radii of the outside cylinder.

2.3.2 Spherical geometry

The analysis of the spherical problem is very similar to that of the cylindrical problem. Instead of the axial component of both stress and strain there is a second azimuthal component which is identical to the first one. In the spherical geometry it is called the tangential component. The elastic strain components are therefore given by

$$\varepsilon_r^{(E)} = \frac{1}{E}[\sigma_r - 2\nu\sigma_t], \tag{108}$$

$$\varepsilon_t^{(E)} = \frac{1}{E}[\sigma_t - \nu(\sigma_r + \sigma_t)], \tag{109}$$

while the thermal strain $\varepsilon^{(T)}$ still follows equ. (73). There is no component which has to be eliminated in order to reduce the number of equations to be solved. After solving equ. (108) and equ. (109) for the two stress components the equilibrium condition for spherical geometry,

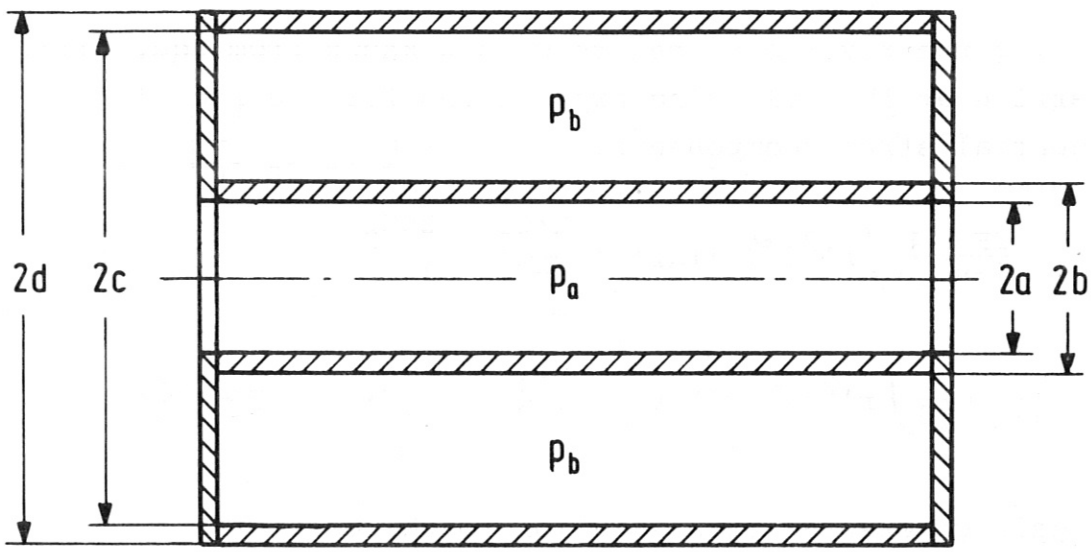

Fig. 6: Cylinder with external pressure load, but free axial expansion

$$\frac{d\sigma_r}{dr} + \frac{2}{r}(\sigma_r - \sigma_t) = 0 \qquad (110)$$

can be applied. With the same compatibility conditions as are valid in the cylindrical case, equs. (84) and (85), the differential equation for the radial displacement can be obtained, the solution of which is

$$u = \frac{1+\nu}{1-\nu} \cdot \alpha \cdot \frac{1}{r^2}\int r'^2 \Delta\vartheta(r')dr' + C_1 r + \frac{C_2}{r^2}. \qquad (111)$$

By doing the reverse procedure with u known from equ. (111) we arrive at the following expressions for the radial and tangential stress components:

$$\sigma_r = -\frac{2E\alpha}{1-\nu}\frac{1}{r^3}\int r'^2 \Delta\vartheta(r')dr' + \frac{E \cdot C_1}{1-2\nu} - \frac{2EC_2}{1+\nu}\cdot\frac{1}{r^3}, \qquad (112)$$

$$\sigma_t = \frac{E\alpha}{1-\nu}\cdot\frac{1}{r^3}\int r'^2 \Delta\vartheta(r')dr' + \frac{EC_1}{1-2\nu} + \frac{EC_2}{1+\nu}\cdot\frac{1}{r^3} - \frac{E\alpha}{1-\nu}\cdot\Delta\vartheta(r). \qquad (113)$$

We again generalize this solution to the case of a hollow sphere with the same boundary conditions as in the case of the cylinder:

$$\sigma_r\ (r=a) = -\ p_a, \qquad (114)$$

$$\sigma_r\ (r=b) = -\ p_b. \qquad (115)$$

By introducing equ. (114) and equ. (115) into equ. (112) and equ. (113) it is possible to evaluate the integration constants C_1 and C_2, yielding

$$C_1 = \frac{(1-2\nu)}{E}\left[\frac{b^3}{b^3-a^3}(p_a-p_b) - p_a\right] +$$

$$+ \frac{1-2\nu}{1-\nu}\cdot\frac{2}{b^3-a^3}\,\alpha\int_a^b r'^2 \Delta\vartheta(r')dr', \qquad (116)$$

$$C_2 = \frac{1+\nu}{2E} \cdot \frac{a^3 b^3}{b^3-a^3} (p_a - p_b) +$$

$$+ \frac{1+\nu}{1-\nu} \cdot \frac{a^3}{b^3-a^3} \cdot \alpha \int_a^b r'^2 \Delta \vartheta(r') dr'. \qquad (117)$$

With C_1 and C_2 from these equations the final results for the radial and tangential stress components σ_r and σ_t, equ. (112) and equ. (113), become

$$\sigma_r = - p_a + (p_a - p_b) \cdot \frac{b^3}{b^3-a^3} \left(1 - \frac{a^3}{r^3}\right) +$$

$$+ \frac{E\alpha}{1-\nu} \left[\frac{r^3-a^3}{b^3-a^3} \cdot \frac{2}{r^3} \int_a^b r'^2 \Delta \vartheta(r') dr' - \frac{2}{r^3} \int_a^r r'^2 \Delta \vartheta(r') dr' \right], \qquad (118)$$

$$\sigma_t = - p_a + (p_a - p_b) \cdot \frac{b^3}{b^3-a^3} \left(1 + \frac{a^3}{2r^3}\right) +$$

$$+ \frac{E\alpha}{1-\nu} \left[\frac{2r^3+a^3}{b^3-a^3} \cdot \frac{1}{r^3} \int_a^b r'^2 \Delta \vartheta(r') dr' + \frac{1}{r^3} \int_a^r r'^2 \Delta \vartheta(r') dr' - \Delta \vartheta(r) \right]. \qquad (119)$$

Again, these equations show the same structure as was indicated in equ. (101) so that an easy splitting into a mechanical and a thermal contribution can be made. The thermal contributions in both equ. (118) and equ. (119) are, furthermore, in complete agreement with Timoshenko [7].

2.3.3 Plane geometry

2.3.3.1 Thermal stress

In the case of plane geometry the three strain components, equ. (69), read

$$\varepsilon_x = \frac{1}{E}[\sigma_x - \nu (\sigma_y + \sigma_z)] + \alpha \Delta \vartheta, \qquad (120)$$

$$\varepsilon_y = \frac{1}{E}\left[\sigma_y - \nu(\sigma_x + \sigma_z)\right] + \alpha\Delta\vartheta, \tag{121}$$

$$\varepsilon_z = \frac{1}{E}\left[\sigma_z - \nu(\sigma_x + \sigma_y)\right] + \alpha\Delta\vartheta. \tag{122}$$

According to fig. 7 it is assumed that there is a temperature distribution in the x-direction which does not, however, vary with y or z. The plate shall be perfectly restrained in the lateral directions y and z,

$$\varepsilon_y = \varepsilon_z = 0, \tag{123}$$

and shall not be loaded by any additional pressure, which means

$$\sigma_x = 0. \tag{124}$$

Then from equs. (120) to (122) the stresses can be directly derived:

$$\sigma_y = \sigma_z = -\frac{E\alpha}{1-\nu}\cdot\Delta\vartheta(x). \tag{125}$$

If, however, the plate is free to expand laterally normal forces and - in the case of a temperature distribution not symmetrical with respect to the y-z plane - even bending moments have to be superposed to arrive at a plate which is free of force. Assuming free expansion in both the y and z-directions, Timoshenko [7] gave the solution

$$\sigma_y = \sigma_z = -\frac{E\alpha}{1-\nu}\cdot\Delta\vartheta(x) + \frac{E\alpha}{1-\nu}\cdot\frac{1}{2c}\int_{-c}^{c}\Delta\vartheta(x)\,dx +$$

$$+\frac{E\alpha}{1-\nu}\cdot\frac{3x}{2c^3}\int_{-c}^{c}x\,\Delta\vartheta(x)\,dx. \tag{126}$$

Since equ. (126) originated from the consideration of forces and moments with respect to a single direction, y or z, it should be possible to use equ. (125) and (126) for the different stress components, if different boundary conditions with regard to expansion are valid. It should be

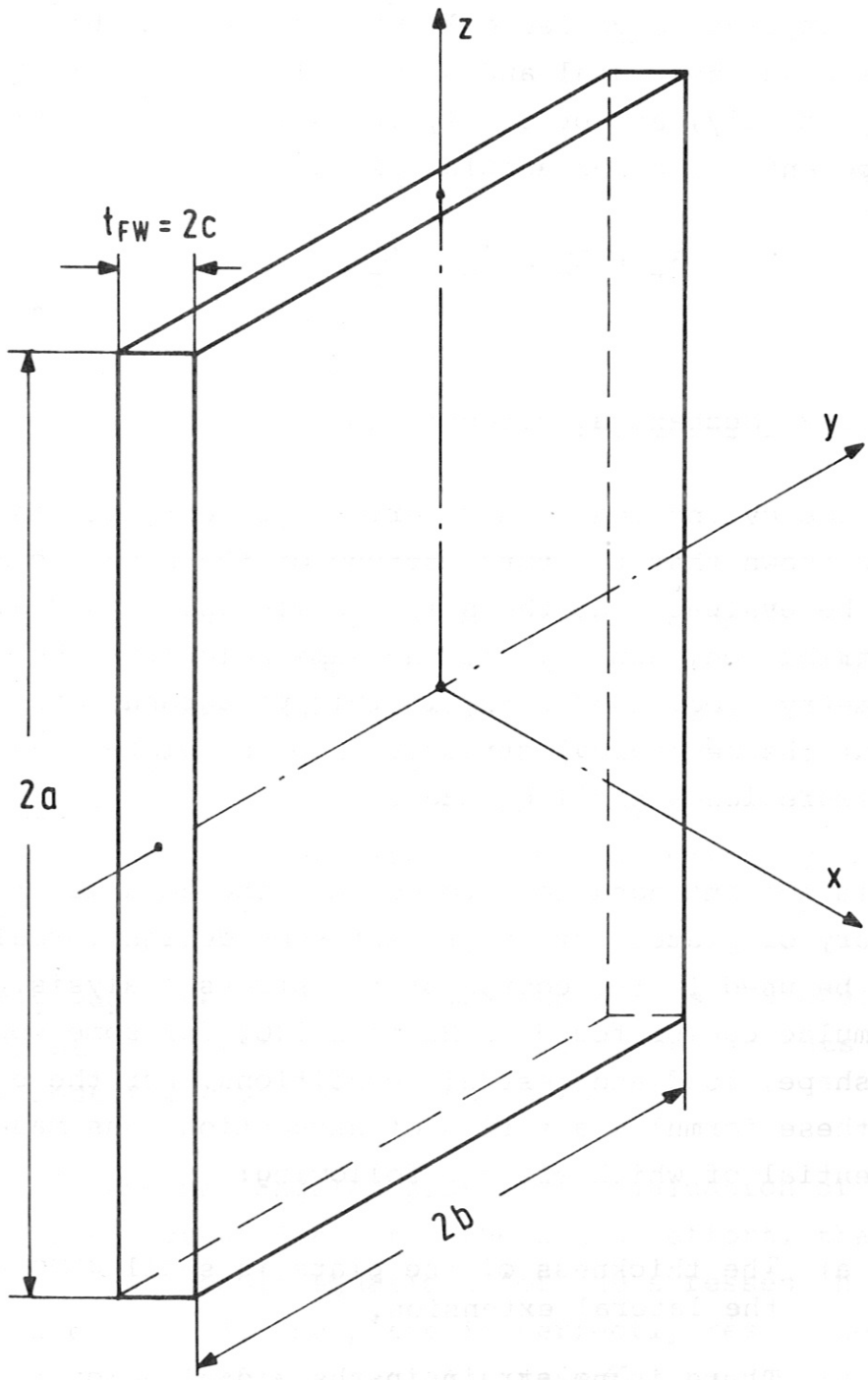

Fig. 7: Further definitions for plane geometry.

mentioned that equ. (125) and equ. (126) were derived for the case of rectangular coordinates. They are, however, applicable in the same way to a circular plate in which the temperature varies only with the axial thickness. In this case the radial and azimuthal stresses, σ_r and σ_θ respectively, are precisely the same as the lateral components in a rectangular plate:

$$\sigma_r = \sigma_\theta = \sigma_y = \sigma_z \tag{127}$$

2.3.3.2 Mechanical stress

For the cylindrical and spherical geometry it has already been shown that the total stress of the single components can be evaluated as the sum of a mechanical and a thermal contribution, equ. (101). The same holds for the plane geometry, too. Therefore, in this paragraph some remarks about the mechanical stresses in plane plates caused by pressure loads shall be made.

It is not intended here to go into the details of the theory of plates but to present some design formulae which can be used in the course of the stress analysis. Such formulae can be found in Hütte I [10] for some special cases of shape, load and restrain conditions. For the evaluation of these formulae a series of assumptions was made the most essential of which are the following:

a) The thickness of the plate is small compared with the lateral extension.

b) There is no strain in the mid-plane of the plate.

c) The stress component in the direction of the thickness of the plate, here designated as σ_x, is small compared with the lateral components.

For the subsequent procedure, the last of these assumptions is converted to the statement:

$$\sigma_x \equiv 0 \tag{128}$$

For a rectangular plate, as shown in fig. 7, with the thickness t_{FW} and the edge length 2a and 2b (a > b) the stresses σ_y and σ_z due to a pressure load Δp can be expressed by the equation

$$\sigma_y = A_y \cdot \Delta p \cdot \frac{b^2}{t_{FW}^2} \tag{129}$$

$$\sigma_z = A_z \cdot \Delta p \cdot \frac{b^2}{t_{FW}^2} \tag{130}$$

The pressure load Δp stands here for the difference:

$$\Delta p = p_a - p_b \tag{131}$$

The coefficients A_y and A_z depend on the ratio b/a and the restrain conditions along the edges. Furthermore, they are a function of both y and z. It can be concluded from [10]that for the case of a laterally perfectly restrained plate the maximum stress occurs at the position $y = \pm b$; $z = 0$. This is in agreement with the results given by Timoshenko et al. [11].

For a simply supported plate the maximum stress obviously [10] occurs at the position $y = z = 0$. The coefficients valid for these two cases are given in fig. 8.

In contrast to the rectangular plate, the evaluation of which calls for a great deal of mathematical effort, there are some more practicable equations for the stresses in a circular plate [10]. If the plate is perfectly restrained along its circumference the radial stress σ_r and the azimuthal stress σ_θ vary with the radius r as

$$\sigma_r = \frac{3 \Delta p \cdot R^2}{8 t_{FW}^2} \left[(1+\nu) - (3+\nu) \frac{r^2}{R^2}\right], \tag{132}$$

$$\sigma_\theta = \frac{3 \Delta p \cdot R^2}{8 t_{FW}^2} \left[(1+\nu) - (1+3\nu) \frac{r^2}{R^2}\right], \tag{133}$$

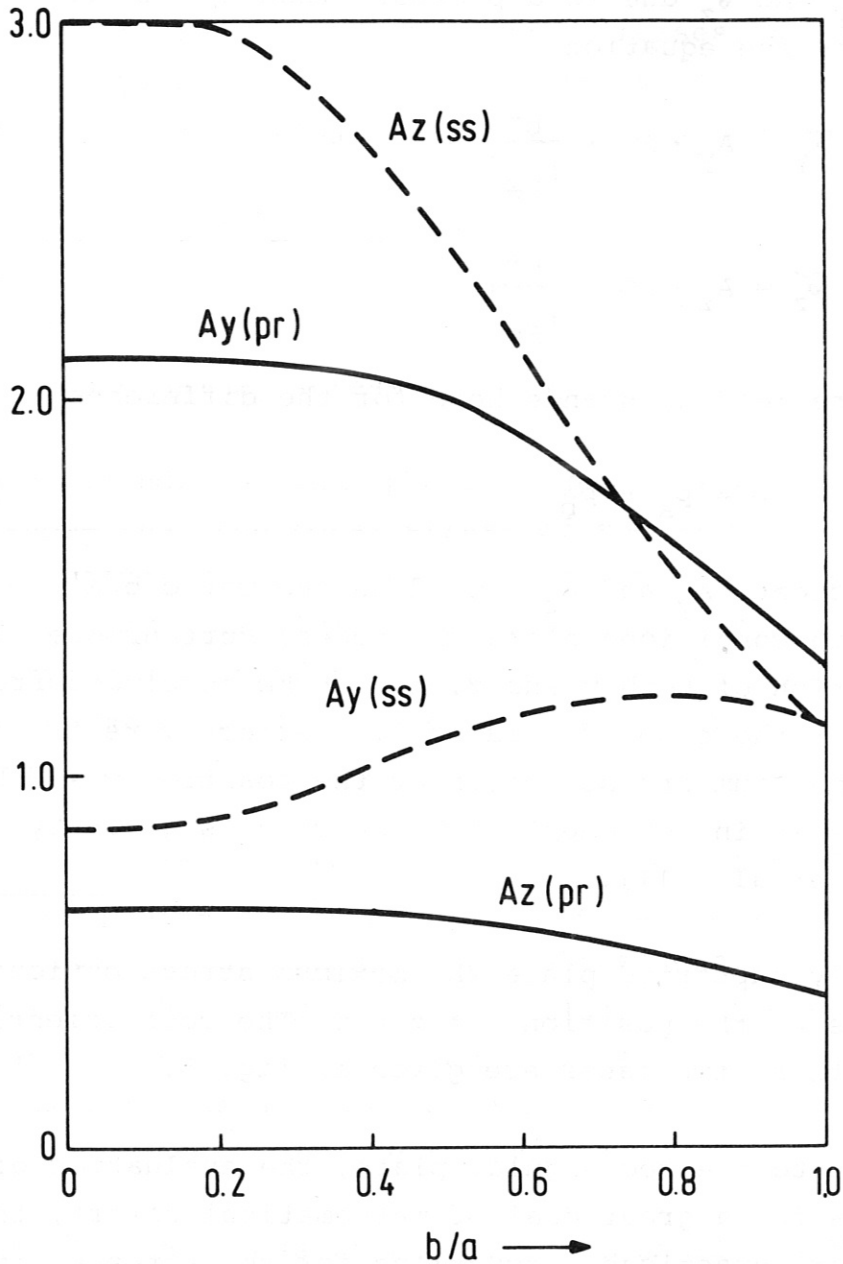

Fig. 8: Coefficients A_y and A_z for the evaluation of the maximum stress in a perfectly restrained (pr) and a simply supported (ss) pressure loaded rectangular plate.

R being the limiting radius of the plate. If the plate is only simply supported the equivalent equations are

$$\sigma_r = \frac{3\,\Delta p \cdot R^2}{8\,t_{FW}^2}\,(3+\nu)\,\left(1-\frac{r^2}{R^2}\right), \tag{134}$$

$$\sigma_\theta = \frac{3\,\Delta p \cdot R^2}{8\,t_{FW}^2}\,\left[(3+\nu) - (1+3\nu)\,\frac{r^2}{R^2}\right]. \tag{135}$$

For the practical purpose of this analysis it is sufficient to calculate the maximum stresses in either case. As can be seen from equ. (134) and equ. (135) the maximum stresses σ_r and σ_θ in the case of the simply supported plate occur at its center and are of equal size:

$$\sigma_{r_{max}} = \sigma_{\theta_{max}} = \frac{3\,\Delta p\,R^2}{8\,t_{FW}^2}\,(3+\nu) \tag{136}$$

In the case of the perfectly restrained plate equ. (132) for the radial stress component yields a tensile maximum at r = 0 and a compressive maximum at r = R. The same holds for the azimuthal stress σ_θ, equ. (133), which,however, yields a lower compressive maximum than that of the radial stress. Since it can be shown that

$$/\sigma_r + \sigma_\theta/_{r=0} = /\sigma_r + \sigma_\theta/_{r\doteq R}\,, \tag{137}$$

$$(\sigma_r + \sigma_\theta)_{r=0} > 0, \tag{138}$$

$$(\sigma_r + \sigma_\theta)_{r=R} < 0, \tag{139}$$

and since it is clear that tensile stresses are more dangerous than compressive stresses of equal size we again choose the values at the center for the further analysis:

$$\sigma_{r_{max}} = \sigma_{\theta_{max}} = \frac{3\,\Delta p\,R^2}{8\,t_{FW}^2}\,(1+\nu). \tag{140}$$

2.3.4 Toroidal geometry

While there is no solution for the problem of thermal stresses in toroidal bodies H. Neuber [12] presented equations for the mechanical stresses in a toroidal shell due to an internal overpressure Δp. With the notation of fig. 9 the azimuthal and the meridional components σ_Θ and σ_ϑ of the stress become

$$\sigma_\Theta = \frac{\Delta p \cdot r_w}{2\, t_{FW}}, \tag{141}$$

$$\sigma_\vartheta = \frac{\Delta p \cdot r_w}{2\, t_{FW}} \; \frac{2R + r_w \sin\vartheta}{R + r_w \sin\vartheta} \,. \tag{142}$$

The maximum meridional stress $\sigma_{\vartheta max}$ occurs, as can easily be concluded from equ. (142), for an angle $\vartheta = -\frac{\pi}{2}$, which means the position at the inside of the toroid. At this location we get

$$\sigma_{\vartheta max} = \frac{\Delta p \cdot r_w}{2\, t_{FW}} \cdot \frac{2R - r_w}{r - r_w} \,. \tag{143}$$

The radial stress component σ_r is set equal to

$$\sigma_r = o \tag{144}$$

which is a necessary assumption in the theory of shells.

For the subsequent analysis we again make use of the principle of superposition of stresses, indicated by equ. (101). Since there are no solutions available for thermal stresses in toroidal geometry we use here as a first approximation those gained for the cylindrical geometry. As the final equations for toroidal shells we therefore use

$$\sigma_r = \frac{E\alpha}{1-\nu}\left[\frac{r^2-a^2}{b^2-a^2}\cdot\frac{1}{r^2}\int_a^b r'\Delta\vartheta(r')dr' - \frac{1}{r^2}\int_a^r r'\Delta\vartheta(r')dr'\right], \tag{145}$$

$$\sigma_\Theta = \frac{\Delta p \cdot (a+b)}{4\,(b-a)} + \frac{E\alpha}{1-\nu}\left[\frac{2\cdot C_R}{b^2-a^2}\int_a^b r'\Delta\vartheta(r')dr' - \Delta\vartheta(r)\right], \tag{146}$$

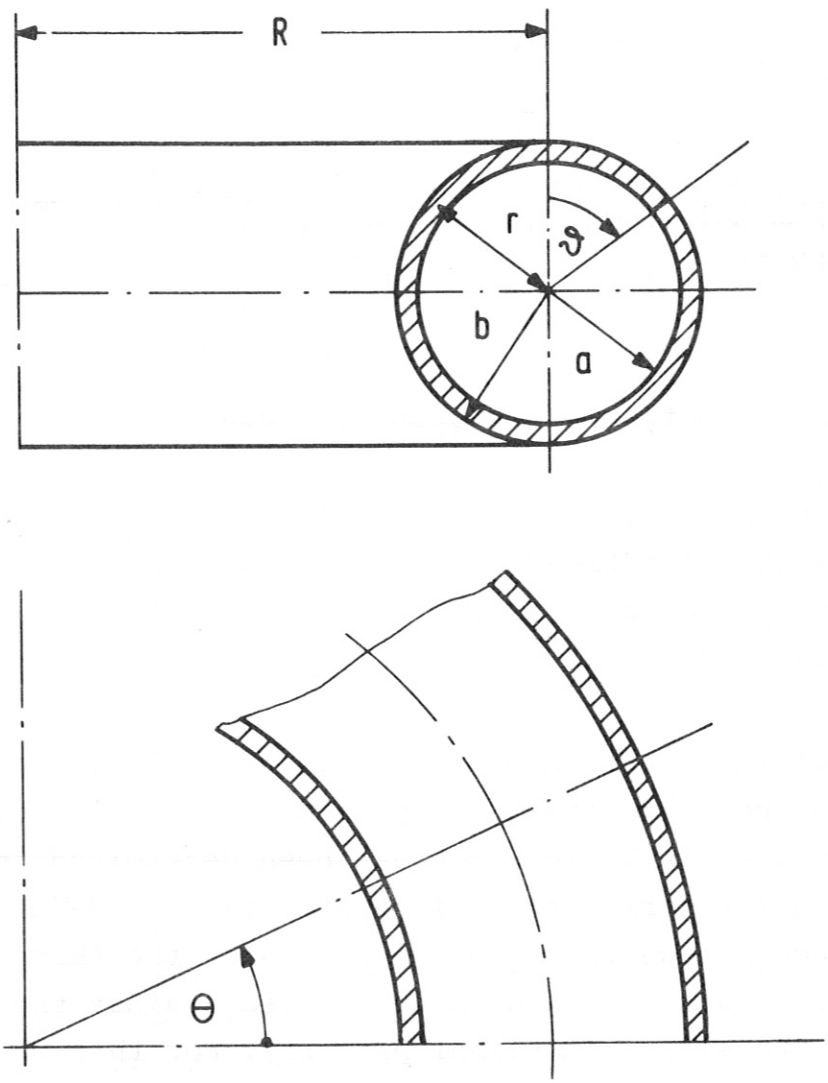

$$r_w = \frac{a+b}{2}$$

$$t_{FW} = b-a$$

Fig. 9: Definitions for toroidal geometry.

with $C_R = \nu$ if the torus shell is perfectly restrained in the "axial" = azimuthal direction,

$C_R = 1$ if it is free to expand,

$$\sigma_\vartheta = \frac{\Delta p\ (a+b)}{4\ (b-a)} \cdot \frac{2\ R - (\frac{a+b}{2})}{R - (\frac{a+b}{2})} +$$

$$+ \frac{E\alpha}{1-\nu}\left[\frac{r^2+a^2}{b^2-a^2}\cdot\frac{1}{r^2}\int_a^b r'\Delta\vartheta(r')dr' + \frac{1}{r^2}\int_a^r r'\Delta\vartheta(r')dr' - \Delta\vartheta(r)\right]. \quad (147)$$

2.3.5 Determination of reference stress

The stress analysis described so far yields three components of stress the directions of which are normal to each other. The question now is whether a certain material can withstand this three-dimensional state of stress.

Aside from real performance tests of accurately specified structural parts, generally only a maximum permissible stress for a material is known which has been determined in a one-dimensional experiment. It is therefore necessary to find a reference stress from the components of the three-dimensional stress which can be quoted against the permissible stress as a material property. For this purpose the field of theoretical mechanics has provided a number of strength hypotheses [10, 12].

The first hypothesis says that the maximum tensile stress is to be used as the reference stress:

$$\sigma_{ref} = \sigma_{max}. \quad (148)$$

It is mostly applied in cases where all three stress components have tensile character.

Due to the second hypothesis the reference stress is determined by the maximum shear stress:

$$\sigma_{ref} = \sigma_{max} - \sigma_{min} = 2\,\tau_{max}. \tag{149}$$

This hypothesis is widely used for ductile materials where deformation or continuously applied loads lead to failure.

In both cases σ_{max} and σ_{min} stand for the maximum and minimum of the three principle stresses σ_I, σ_{II}, and σ_{III}, respectively.

The third hypothesis, which is recommended as the better alternative to the second one, again uses a shear stress as the reference stress. In contrast to the former hypothesis, this one uses the stress occurring in the plane whose surface normal forms angles of equal size with the directions of the three principal stresses σ_I, σ_{II}, σ_{III}. The reference stress resulting from this "octahedral shear stress" is defined as

$$\sigma_{ref} = \sqrt{\frac{1}{2}\left[(\sigma_I - \sigma_{II})^2 + (\sigma_{II} - \sigma_{III})^2 + (\sigma_{III} - \sigma_I)^2\right]}. \tag{150}$$

In general, the principal stresses follow from the components of normal stress and any shear stresses existing by choosing a new coordinate system (I, II, III) such that the shear stresses become zero. Since the present analysis assumes only hydrostatic pressures as the external load with the consequence that shear stresses are not present, the three stress components evaluated for each type of geometry automatically coincide with the principal stresses.

By using the reference stress σ_{ref} it is also possible to define a reference strain ε_{ref} [10]

$$\varepsilon_{ref} = \frac{\sigma_{ref}}{E}. \tag{151}$$

H. Neuber [12], however, recommends that equations equivalent to those for determining the reference stress be used for the reference strain.

In the case of the "normal stress hypothesis",

$$\varepsilon_{ref} = \varepsilon_{max}. \tag{152}$$

In the case of the "shear stress hypothesis",

$$\varepsilon_{ref} = \frac{1}{1-\nu} (\varepsilon_{max} - \varepsilon_{min}) \tag{153}$$

In the case of the "octahedral shear stress hypothesis",

$$\varepsilon_{ref} = \frac{1}{1+\nu} \sqrt{\frac{1}{2} [(\varepsilon_I - \varepsilon_{II})^2 + (\varepsilon_{II} - \varepsilon_{III})^2 + (\varepsilon_{III} - \varepsilon_I)^2]}. \tag{154}$$

Here, as was the case for the stresses, ε_I, ε_{II}, and ε_{III} are the components of strain in the directions of the three principal stresses, ε_{max} and ε_{min} being the maximum and minimum from these principal strains.

2.4 Lifetime profile

Since the analysis described so far yields as the final results the temperature and stress load profiles under steady-state conditions, it is possible to estimate the lifetime of a material exposed to those conditions. This can be done by quoting the temperature and stress versus the time rupture strength of the material under consideration.

This material property takes into account the well-known feature that a slowly rising plastic deformation takes place at high temperatures and high stresses. This mechanism, called thermal creep, is responsible for a limitation of the useful life even at stresses far below the yield strength.

Generally, the literature presents data which indicate a certain limiting stress $\sigma_{B/t}(T)$ a material was able to stand at a certain temperature T for a certain period of time t. For many materials, especially steels, data for $\sigma_{B/10000\ h}$ and a few for $\sigma_{B/100\ 000\ h}$ are known. After the investigation of a lot of experimental data it could be shown [13] that a variety of data $\sigma_{B/t}$ can commonly be represented as a function of a parameter P

$$P = T\ (C + \log t)\,, \tag{155}$$

which is called the Larson-Miller parameter after its originators [13]. This quantity combines the temperature T[K], the operating time t [h], and a material constant C.

By inverting equ. (155) it is possible to obtain the expected lifetime t

$$t = 10^{(P/T - C)} \tag{156}$$

as a function of the absolute temperature T and the Larson-Miller parameter P.

For many materials the time rupture strength $\sigma_{B/t}$ is known as a function of P. By inverting this dependence, a certain value for P can be assigned to a given reference stress σ_{ref}. If this value of P and the temperature T is now introduced in equ. (156), we finally find the lifetime t as a function of T and σ_{ref}: $t = t(T, \sigma_{ref})$.

If lifetimes are calculated by the method just described, as is done in our analysis, a few remarks are necessary to put the results to be expected from this procedure into the right perspective.

- It is not intended to conclude from these results that the fusion reactor first wall will stand the time evaluated even approximately. The author is very well

aware of the fact that there are other mechanisms that contribute to shortening the useful life. The most essential of them may be the degradation of mechanical properties like time rupture strength and ductility by irradiation effects and the most probable need for operating the reactor in a pulsed mode.

- The last step of this analysis - quotation of stress and temperature versus time rupture strength - is, in fact, an inconsistency of the analysis. The time rupture behaviour includes thermal creep, whilst the analysis does not cope with elongations caused by creep. To exclude this inconsistency will be one of the next steps.

- It should be noted that the accuracy of the lifetime estimated by the procedure described here is necessarily very poor. This is a consequence of the appreciable error bars which appear if experimental data $\sigma_{B/t}(P)$ are represented by a smooth curve for the purpose of interpolation. The size of these errors determine, on the other hand, the error of the logarithm of the useful life. It should, therefore, be clear that the determination of lifetimes in the course of this restricted analysis does not aim at absolute values but rather at the detection of tendencies and maybe for comparisons of different materials.

3. COMPUTER PROGRAM

The equations resulting from the mathematical procedure described in the preceeding section have been programmed for the computer. The author's aim in doing this was to arrive at a program structure which permits a twofold kind of usage. At first, a number of basic investigations should be possible showing the influence of simplifying assumptions on the final results. Secondly,

the structure should permit at least parts of the program to become constituents of a modular fusion reactor systems program. These requirements have been met by choosing a structure as is indicated by fig.10.

Four subroutines, QPRF, PFRF, SPRF, and LPRF,have been elaborated which calculate the profiles of power density, temperature, stress, and lifetime, respectively. Three of them need further subprograms,the function of which is described below. The four main subroutines are connected to each other by a main program which, at present, serves for the purpose of testing. It can easily be replaced by any other main program prescribing a different strategy.

3.1 Main program

The main program in operation at present has been written especially for test purposes. It performs all input and output operations.

The following quantities are needed for input:

MTRL	material identification number (see: a))
MOD	geometry option
	= - 2 spherical, convex curvature
	= - 1 cylindrical, convex curvature
	= 0 plane
	= 1 cylindrical, concave curvature
	= 2 spherical, concave curvature
	= 3 toroidal
MQ	number of available intervals (see b))
NP	number of intervals desired (see b))
ISO	option for stress evaluation (see c))
	= 0 axial or lateral elongation prevented
	= 1 axial or lateral elongation permitted
IS1	option for thermal stress evaluation (see c))
	= 0 no stresses at low temperature TO
	= 1 no stresses at average wall temperature TM

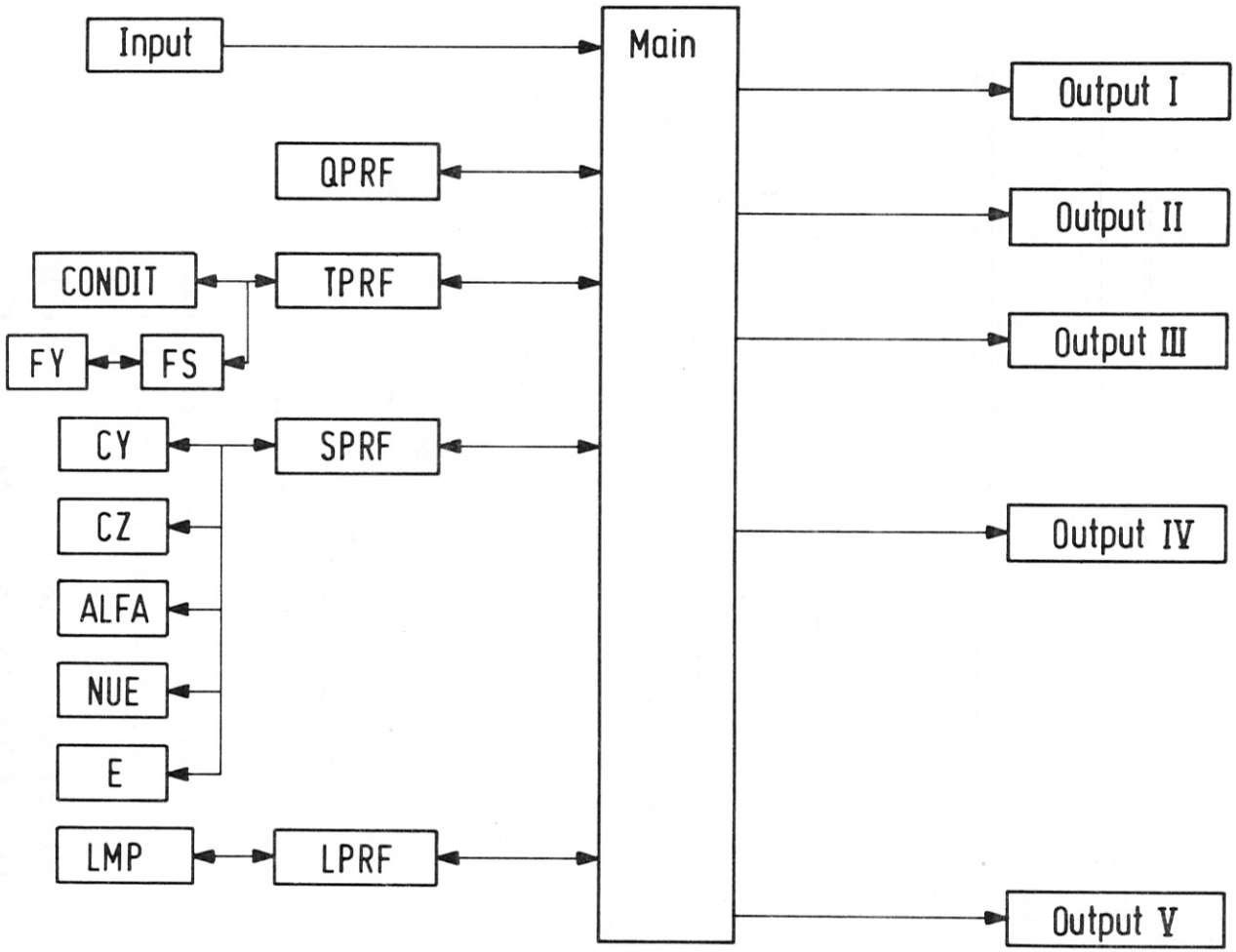

Fig. 10: Program structure

IS2 option for thermal stress evaluation (see c))
= 0 E, ν, and α temperature independent
= 1 E, ν, and α temperature dependent

IS3 option for reference stress evaluation (see c))
strength hypothesis to be applied is:
= 0 normal stress
= 1 maximum shear stress
= 2 octahedral shear stress

RT torus radius [cm]

RW wall radius [cm]

TFW wall thickness [cm]

TB thickness of breeding zone [cm]

HD half thickness for radiation absorption [cm] (see d))

PWN neutron wall loading [W/cm^2]

PWS radiation wall loading [W/cm^2]

TO wall temperature at the cool side [C]

PIN wall inside pressure [bar]

PAU wall outside pressure [bar]

RA outer radius of cylinder or sphere in the case MOD > 0 [cm]
radius of circular plate for MOD = 0 [cm]
(see e)

AA, BB } edge lengths of rectangular plate [cm]
for MOD = 0; BB < AA
(see e)

QN power density by interval due to neutron reactions [W/cm^2] (MQ values)

QG power density by interval due to gamma reactions [W/cm^2] (MQ values)

DX widths of intervals [cm] (MQ values)

For a better understanding a few remarks are added:

a) MTRL: material identification number

Since this type of analysis should not be restricted to a single material provision was made to store material data for various materials in the subprograms CONDIT, ALFA, NUE, E, and LMP. To distinguish these data, the identification number MTRL, which is a four-digit integer number, was introduced. To obtain some order in the variety of metals and alloys to be considered it was decided to choose as the first two digits the charge number of that element most abundant in the alloy. The last two digits are consecutively assigned to special alloys. The following numbers have already been assigned:

MTRL	material specification
2601	1.4970 stainless steel
	≙ Sandvik 12R72HV
2602	1.4988 stainless steel
2603	1.4961 stainless steel
2604	1.4981 stainless steel
2605	1.4436 stainless steel
2606	1.4919 stainless steel
2607	316 SS stainless steel
2801	Incolloy 800
2802	Inconel 625
2803	Hastelloy X
2804	Inconel 718

Assignment of a material identification number does not, however, automatically mean complete availability of data. Table II shows the present status of the subprograms containing the information on the material properties. The data included in these programs are taken from K.D. Closs [14] and K. Ehrlich [15].

Table II: Present status of the material properties subprograms.

MTRL	CONDIT	ALFA	E	NUE	LMP	Material
2601	1	1	1	1	1	1.4970
2602	1	1	1	1	0	1.4988
2603	1	1	1	1	0	1.4961
2604	1	1	1	1	0	1.4981
2605	1	1	1	1	0	1.4436
2606	1	1	1	1	0	1.4919
2607	1	1	1	1	0	316 SS
2801	1	1	1	1	0	Incolloy 800
2802	1	1	1	1	0	Inconel 625
2803	1	1	1	1	0	Hastellog X
2804	1	1	1	1	0	Inconel 718

0 not available

1 available

b) MQ, NP: number of intervals

The program is constructed to start from the results of a neutronics/photonics calculation. This type of calculation yields the power density due to neutron reactions, QN(M), and that due to gamma reactions, QG(M), in a limited number, MQ, of arbitrarily sized, DX(M), intervals. Usually, MQ does not exceed MQ = 10, which is too few for the purpose of numerical integration that has to be applied in this analysis. Therefore the entire wall is subdivided into a number NP of now equally sized intervals.

c) ISO, IS1, IS2, IS3: options for stress evaluation

For stress evaluation a number of options have been introduced essentially for test purposes. While ISO is left to the user's discretion, IS1 should usually be chosen to be IS1 = 1, and IS3 should be IS3 = 2. The influence of the choice of IS2 will be shown below.

d) HD: half thickness for radiation absorption

As was already outlined in section 2.1,the wall depth HD at which the power density due to radiation absorption has decreased to half the value at the surface exposed to the plasma depends upon the spectral distribution of the radiation energy. At this stage of the analysis the influence of the size of HD upon the characteristic results should be identified. Thus, HD is used as a free input quantity.

e) RA, AA, BB: additional quantities describing the geometry

If MOD > 0, TFW and RW and in the case MOD = 3 additionally RT are capable of describing the geometry completely. In this case, RA, AA, and BB do not have any meaning.

If MOD < 0, however, additional information is necessary to describe the relation between the entire toroid and a single module. Of the two possibilities of doing this - either the number or the sizes of modules can be

fixed - the latter was chosen. RA, therefore, defines the outer radius of the cylinder or sphere limiting the module at the side exposed to the plasma. AA and BB do not have any meaning.

If MOD = 0, there is a possibility of deciding between the assumption of a circular or a rectangular plate of thickness TFW. If a circular plate is chosen, RA has to be set equal to the outer radius of the plate; AA and BB have to be zero. In the case of a rectangular plate AA and BB have to be set equal to the side lengths of the plate; RA has to be set equal to zero.

Owing to fig. 10 the operation sequence of the main program is very simple. When the input data for the first example has been read, a first output list (Output I) is produced which contains all necessary information about the input. Then subsequently the four main routines QPRF, TPRF, SPRF and LPRF are called for operation. Every time one of these routines has finished the main program edits the profiles of the most interesting quantities just evaluated. Thus, the single output lists contain the following information:

Output II:	Nuclear power density profile	QQN(N)
	Radiation power density profile	QQS(N)
	Total power density profile	Q(N)
Output III:	Total power density profile	Q(N)
	Heat flux potential profile	S(N)
	Temperature profile	T(N)
	Profile of temperature difference	(T(N) - TO)
Output IV:	Profiles of the three components of mechanical stress	SM(I,N)
	Profiles of the three components of thermal stress	ST(I,N)
	Profiles of the three components of total stress	SP(I,N)
	Reference stress profile	SV(N)

Output V:	Total power density profile	Q(N)
	Temperature profile	T(N)
	Reference stress profile	SV(N)
	Lifetime profile	LD(N)

After complete evaluation of the first example the next can be directly attached by defining a completely new input data block.

3.2 The subroutine QPRF

The task of this subroutine,which is to establish a power density profile at NP locations equally distributed across the wall thickness,is accomplished in three steps.

First the nuclear power density profile is calculated. By adding neutron induced and gamma induced power density by macro-interval the total nuclear power density by macro-interval is calculated. By means of an interpolation procedure the power density values at both surfaces and in the middle of the wall are determined, which are then used to define the coefficients q_{no}, a, and b of equ. (1). These coefficients are used to calculate the NP profile values.

The second step is to evaluate the radiation power density profile. From the radiation wall loading PWS and the arbitrarily chosen half-thickness HD μ and q_{bo}, the coefficients of equ. (2) are calculated. This equation then is used to evaluate all NP profile values.

Addition of the nuclear and radiation power density profiles completes the work of this subroutine. Both the profiles and the coefficients mentioned above are transferred to the main program.

3.3 The subroutine TPRF

The operation of this subroutine starts by establishing a table in which temperatures and heat flux potentials for the material under consideration are assigned. This is done using the function subprogram CONDIT.

To evaluate the heat flux potential for every interval, equs. (35), (34), and equ. (33) have to be used subsequently. Since the program is, at present, fixed to the power density profile defined by equ. (36),the first integration, equ. (35), can be done analytically. The corresponding functions are contained in the function subprogram FY. The second integration, however, which is indicated by equ. (34) has to be done numerically. The discrete values of the function to be integrated are supplied by the function subprogram FS, while the integration itself is done by using the method of Simpson. Now the profile of the heat flux potential can be established. By inverse interpolation in the table produced on starting this routine the heat flux potential profile is converted to the temperature profile.

3.4 The subroutine SPRF

This subroutine starts with the evaluation of the average wall temperature which is needed for the determination of some material properties. As the next operation the calculation of the mechanical stresses due to the pressure loads follows. This calculation is done by using the different formulas described above,depending on the geometry (MOD) and on the restrain condition (ISO) used.

When this part of the calculation is completed, the evaluation of thermal stresses is started. Depending on the option IS1,the temperature differences are fixed and, if IS2 = 1,multiplied by the temperature dependent materials properties factors. The integrations necessary to obtain

the stresses from the temperature differences are again performed numerically using Simpson's rule.

Finally, the three components of mechanical and those of thermal stress are added to yield the components of three-dimensional total stress. Owing to the choice of IS3 these stress components are subjected to the equivalent strength hypothesis to yield the reference stress profile.

Subroutine SPRF makes use of five function subprograms. CY and CZ contain the factors A_y and A_z respectively used to evaluate the stress components due to equ. (129) and equ. (130) for the rectangular plate. ALFA, NUE, and E are subprograms from which thermal expansion, Poisson's ratio, and Young's modulus are called.

3.5 The subroutine LPRF

The very short routine LPRF finally takes for every point of the profile both temperature and reference stress in order to estimate a lifetime.

The reference stress is fed to the subroutine LMP, which provides the Larson-Miller parameter P valid for the case that the reference stress is just the rupture strength belonging to this parameter value. LMP additionally supplies the material constant C and the maximum short time rupture strength SMAX, which is an absolute limit yielding a zero lifetime.

From the Larson-Miller parameter and the temperature the lifetime t is derived using the constant C.

4. FIRST RESULTS OF BASIC INVESTIGATIONS

It is very likely that the further analysis of the problem of the mechanical performance of the first wall will necessitate one or another simplification in order to arrive at operable solutions. By means of the program developed here it is possible to check the consequences of such simplifications at least as far as the steady state behaviour is concerned.

Some of the simplifications possibly needed can already be foreseen. They have been investigated at least for a single set of parameters and the results are reported in the subsequent sections.

For all calculations a temperature of 500 C was assumed at the cool side of the wall, the material considered is 1.4970 stainless steel, and for reference stress calculation the octahedral shear stress has been used for the strength hypothesis.

4.1 Influence of the shape of the nuclear power density profile

The approximation of the nuclear power density profile by equ. (1) followed from the first neutronics/photonics calculations for a niobium first wall performed at our laboratory. Subsequent systematic evaluations of liquid lithium/stainless steel blankets [4] showed, in principle, the same dependence though much closer to linearity. Therefore, the assumption of a linear profile may be justified if any difficulties should occur in the analysis using equ. (1) in its original form. A further simplification, finally, would be to assume a constant power density in the wall as is often done in reactor studies.

For a special example we evaluated the three cases in order to see the consequences in the final results. To see

clear differences we chose a 2 cm thick stainless steel wall which is exposed to a neutron wall loading of P_N = 100 W/cm^2. The power density profile shown in fig. 11 and designated as curve "a" is that which follows from the approximation of the neutronics/photonics results by equ. (1) in its original form. Curve "b" is a linear approximation, and curve "c" the constant power density case, both evaluated with regard to agreement in the total amount of heat generation in the wall.

To evaluate temperatures, stresses and lifetimes,it is necessary to make further assumptions. For this investigation a hollow sphere with an outer radius of 30 cm was assumed, this outer surface being exposed to the plasma (MOD =-2). Plasma radiation was excluded (PWS = 0.) as was an extra pressure load (PIN = PAU).

Table III shows the essential results of these calculations. As far as temperatures and stresses are concerned,there is nearly no difference between the cases "a" and "b". The deviation of case "b" as compared to case "a" is positive and is below 0.5 %. The assumption of a constant power density, case "c", however, causes deviations of the order of 5 % which additionally tend to the negative side. This means an underprediction of temperatures and stresses.

The relatively small differences in temperatures and stresses are responsible, as was already outlined in section 2.4, for very big differences in the estimated time rupture life. This is underlined by the results shown in table III. What can be stated with certainty for the case considered here is that the life of the first wall under steady-state conditions would be limited by the temperature/stress condition at the hot surface of the wall although the reference stress is only half that occurring at the cooler surface.

According to the results for temperatures and stresses the minimum life is predicted by case "b", the linear

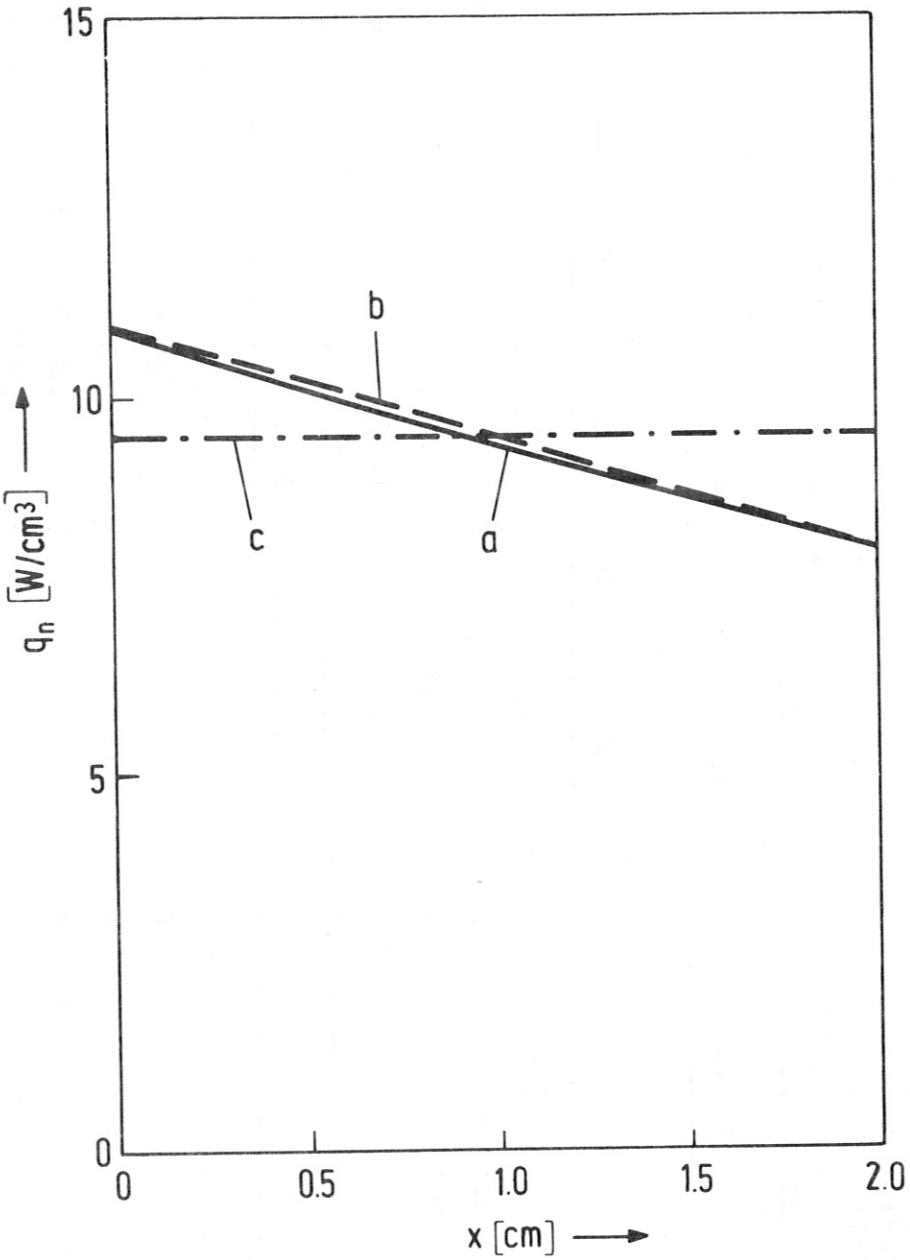

Fig. 11: Nuclear power density profiles in a stainless steel first wall
a) real profile,
b) linear approximation,
c) constant power density.

Table III: Results of calculations showing the influence of the shape of the nuclear power density profile $q_n(x)$.

Assumptions:			
Neutron wall loading	PWN	= 100	W/cm^2
Radiation wall loading	PWS	= 0.	
Half thickness	HD	= 0.	
Wall thickness	TFW	= 2.	cm
Pressure load	PIN-PAU	= 0.	
Geometry	MOD	= -2	(spherical convex)
Radius of Sphere	RA	= 30	cm

	"a" real profile	"b" linear profile	"c" const.pow.den.
Temperature difference across wall [C]	101.79	102.25	97.15
Temperature at hot surface [C]	601.79	602.25	597.15
Reference stress at hot surface [kp/cm^2]	1221.24	1226.91	1139.37
Lifetime at hot surface [h]	$1.738 \cdot 10^7$	$1.585 \cdot 10^7$	$5.466 \cdot 10^7$
Reference stress at cold surface [kp/cm^2]	2571.81	2582.84	2485.35
Lifetime at cold surface [h]	$4.146 \cdot 10^7$	$3.881 \cdot 10^7$	$7.030 \cdot 10^7$
Deviation in temperature difference	0.	+ 0.45 %	- 4.56 %
" " ref.stress at hot surface	0.	+ 0.46 %	- 6.7o %
" " " " at cold surface	0.	+ 0.43 %	- 3.36 %
" " lifetime at hot surface	0.	- 8.8 %	+ 214.5 %
" " " " cold surface	0.	- 6.39 %	+ 69.6 %

approximation. It should, therefore, be sufficient to base further calculations on this assumption rather than on a constant power density,to remain on the safe side.

To gain an impression about the real profiles occurring in the wall and the deviations caused by assuming a constant power density the temperature, stress, and life profiles have been plotted in figs. 12, 13, and 14, respectively.

The temperature profile, fig. 12, shows the typical, nearly parabolic shape characteristic of walls with internal heat sources.

The stress profile, fig. 13, characterized by the variation of the tangential stress σ_t, shows tensile stresses at the cold surface and compressive stresses at the hot one. Also shown in this picture is the variation of the reference stress σ_{ref}. While in the tensile region of σ_t σ_{ref} coincides with the tangential stress, σ_{ref} is evaluated to be $\sigma_{ref} = -\sigma_t$ in the compressive region of σ_t. For this reason two maxima occur at the two surfaces of the wall. Which of these maxima is more dangerous with respect to the lifetime depends upon the temperature. In the case evaluated here it is the combination at the hot surface as can be seen from the lifetime profile, in fig. 14.

In fig. 13 a straight line (-·-·-) has been additionally drawn. This line characterizes the thermal stress distribution following from the approximation usually applied [1, 2, 3]:

$$\sigma_{th} = \pm \frac{E\alpha}{1-\nu} \cdot \frac{\Delta\vartheta}{2} \qquad (157)$$

This approximation says that the thermal stresses at the hot and the cold surface are of equal size but different sign, the size being given by half the temperature difference between the two surfaces. In between, a linear stress distribution is normally assumed.

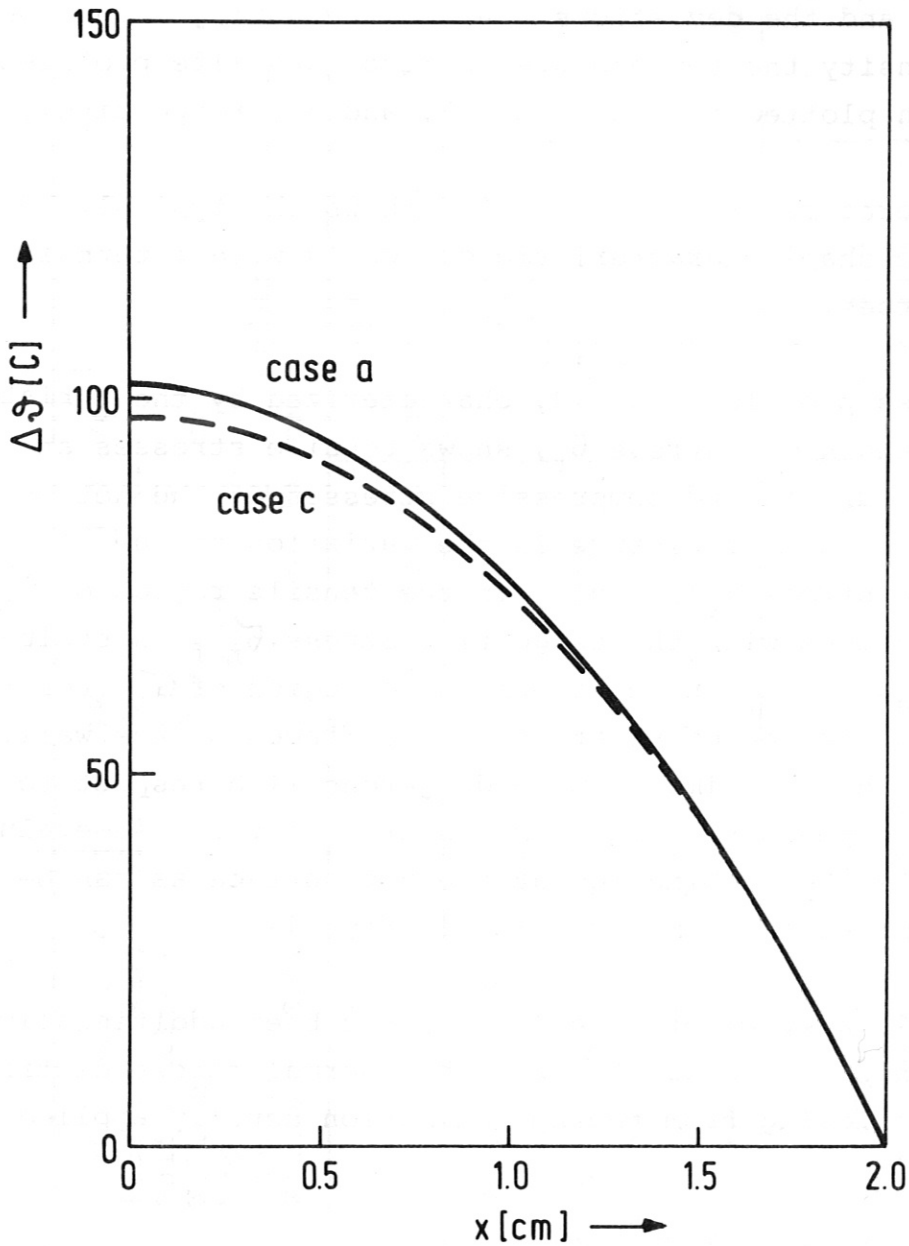

Fig. 12: Temperature profile for real (case a) and constant (case c) power density distribution.

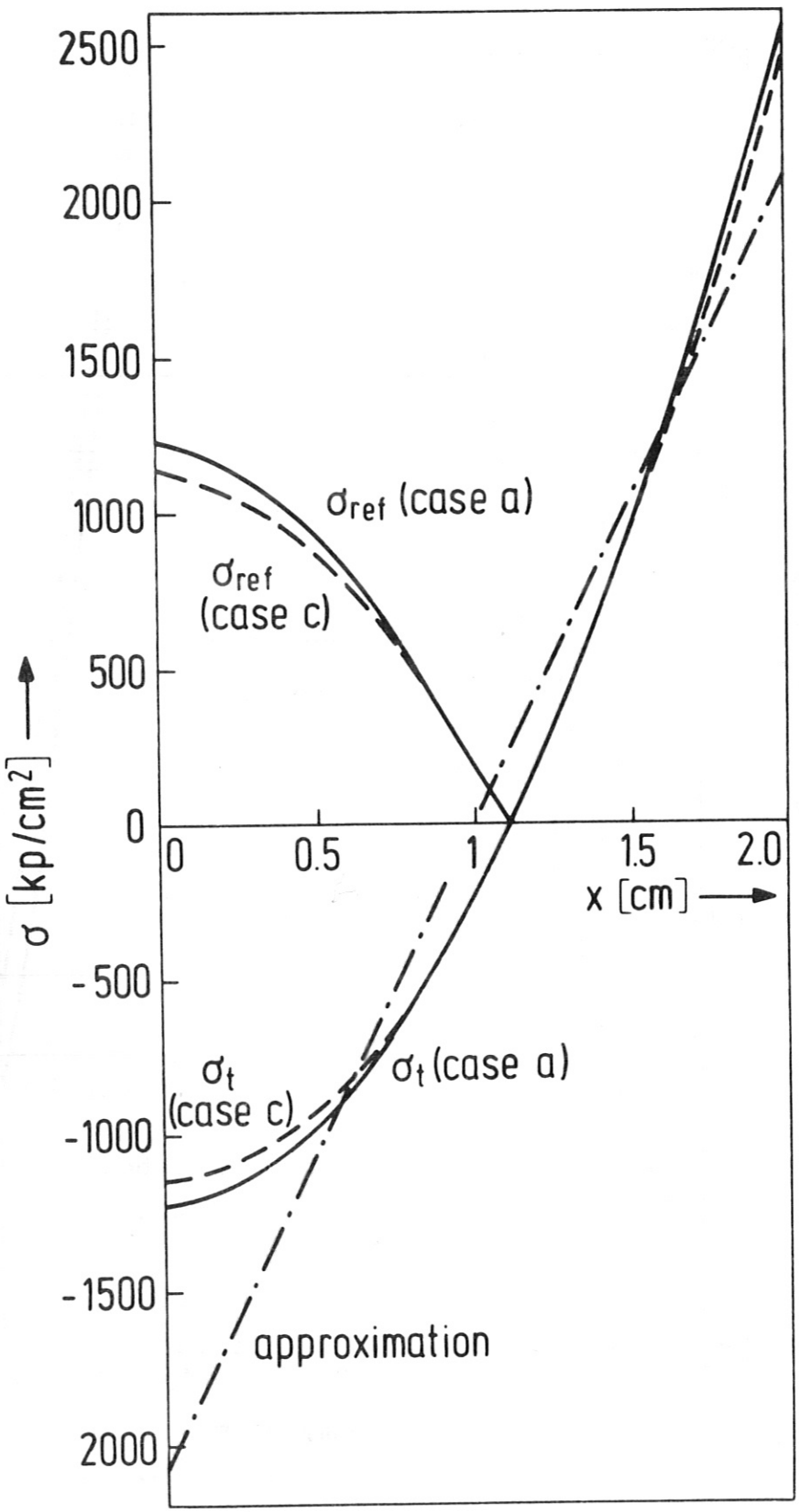

Fig. 13: Stress profile for real (case a) and constant (case c) power density distribution and for an approximation usually applied (-·-·-).

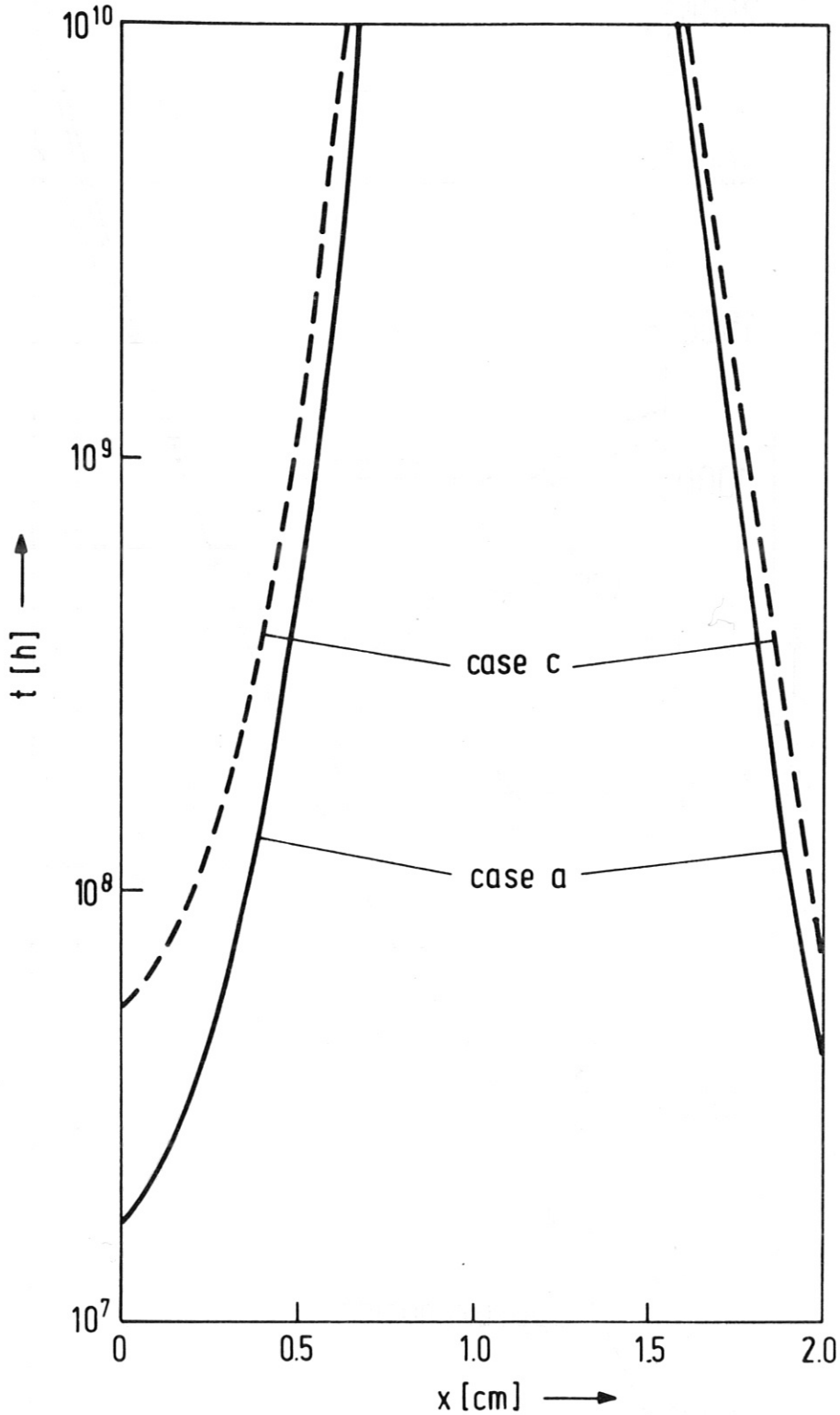

Fig. 14: Lifetime profile for real (case a) and constant (case c) power density distribution.

All these assumptions coincide with the case of plane geometry, perfect restraining of the plate and a linear variation of temperature across the wall such that the average temperature can be assumed to be located in the middle of the wall.

It is most probable that the approximation of assuming plane geometry throughout may be justified. The assumption of a linear variation of the temperature, however, means that there are no internal heat sources in the wall. Such an assumption is simply wrong and leads, as can be seen from fig. 13, to results far from reality.

From the evaluation above it already followed that the critical surface is the hot one, characterized by $\vartheta \approx 602$ C and $\sigma_{ref} \approx 1220$ kp/cm^2. The approximation just described yields for the same temperature a reference stress of $\sigma_{ref} \approx 2070$ kp/cm^2. These data quoted versus the time rupture properties would result in a lifetime of about $6 \cdot 10^5$ h instead of $1.7 \cdot 10^7$ h.

4.2 Influence of the shape of the radiation power density profile

As was outlined in section 2.1, the radiation originating from the plasma will be absorbed in the first wall and converted to heat. The resulting power density profile depends essentially on the radiation energy spectrum. Usually it is assumed that this energy is deposited within a very thin surface layer so that it can be treated as an external heat flux. By means of the computer program described in section 3 it has been studied what consequences arise from this assumption.

Again, a 2 cm thick stainless steel wall has been considered which is exposed to a neutron wall loading of $P_n = 100$ W/cm^2, resulting in a nuclear power density of

approximately 10 W/cm^3. Now a radiation wall loading of P_B = 5 W/cm^2 has been additionally superimposed. The resulting radiation power density profiles are shown in fig. 15,depending on the choice of the half thickness h. In the calculations h was varied between 0.5 cm and 0, the latter meaning that there are no heat sources due to radiation inside the wall but all heat enters the wall by heat conduction.

The results of these calculations are summarized in table IV. Depending on the choice of the half thickness h,the temperature difference between the hot and the cold surface differs appreciably. The assumption of all radiation heat entering from outside causes the biggest temperature differences. The deeper the radiation penetrates into the wall the lower will the temperature peak be.

The temperature profiles for the two limiting cases, h = 0 and h = 0.5 cm, are shown in fig. 16 together with the profile for pure nuclear heating. It can be recognized that again the region near the hot surface is most influenced by the choice of h. In the parameter range investigated the deviations in the temperature difference amount to about 10 %.

This situation is underlined by the results for the reference stress and the calculated life shown in tableIV.Whilst the maximum difference in the reference stress is about 4.5 % at the cold surface, it amounts to about 19 % at the hot surface. The equivalent differences in the calculated lifetime are factors of 2 at the cold, but 32 at the hot surface.

These differences should not, however, be overemphasized because we feel that the real deposition depth of plasma radiation will be rather in the neighbourhood of h = 0 than at h = 0.5 cm. We therefore want to argue vice versa

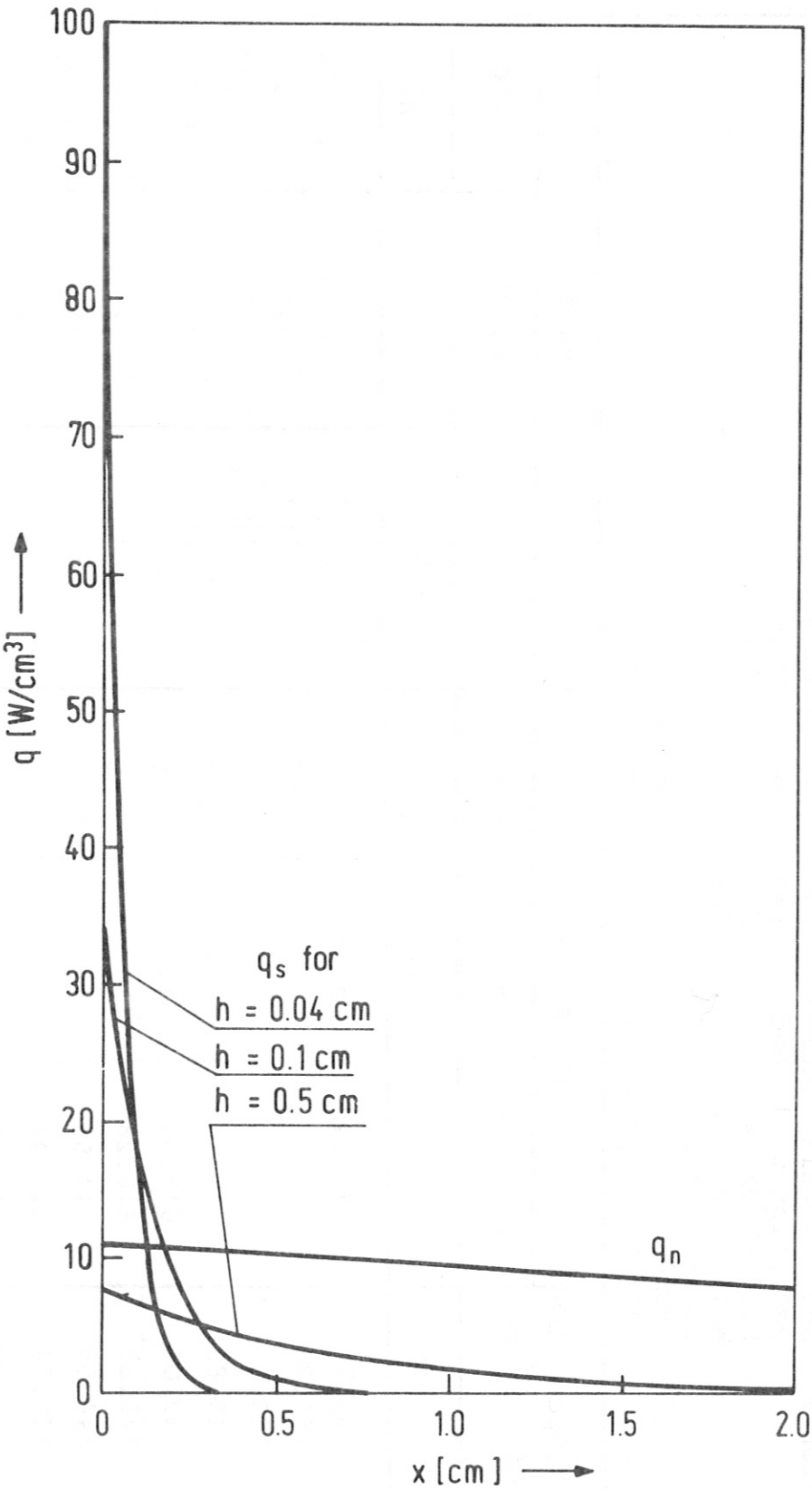

Fig. 15: Radiation power density profiles for $P_B = 5\ W/cm^2$ for various half thicknesses h.

Table IV: Results of calculations showing the influence of the shape of the radiation power density profile $q_b(x)$.

Assumptions:			
Neutron wall loading	PWN	= 100	W/cm^2
Radiation wall loading	PWS	= 5	W/cm^2
Half thickness	HD	= h	(varied)
Wall thickness	TFW	= 2	cm
Pressure load	PIN-PAU	= 0.	
Geometry	MOD	= -2	(spher., convex)
Radius of sphere	RA	= 30	cm

h	temperature difference	hot surface			cold surface		
		temperature	ref.stress	life	temperature	ref. stress	life
[cm]	[°C]	[°C]	[kp/cm^2]	[h]	[°C]	[kp/cm^2]	[h]
0.	151.94	651.94	2066	846	500.	3515	325 800
0.02	151.33	651.33	2046	995	500.	3513	328 900
0.04	150.56	650.56	2021	1218	500.	3510	333 000
0.06	149.80	649.80	1997	1488	500.	3506	338 300
0.08	149.04	649.04	1974	1811	500.	3502	344 700
0.10	148.28	648.28	1951	2196	500.	3497	352 200
0.20	144.59	644.59	1852	5269	500.	3463	408 300
0.30	141.34	641.34	1777	10660	500.	3423	489 000
0.40	138.80	638.80	1722	18270	500.	3387	576 600
0.50	136.88	636.88	1683	27340	500.	3357	659 700

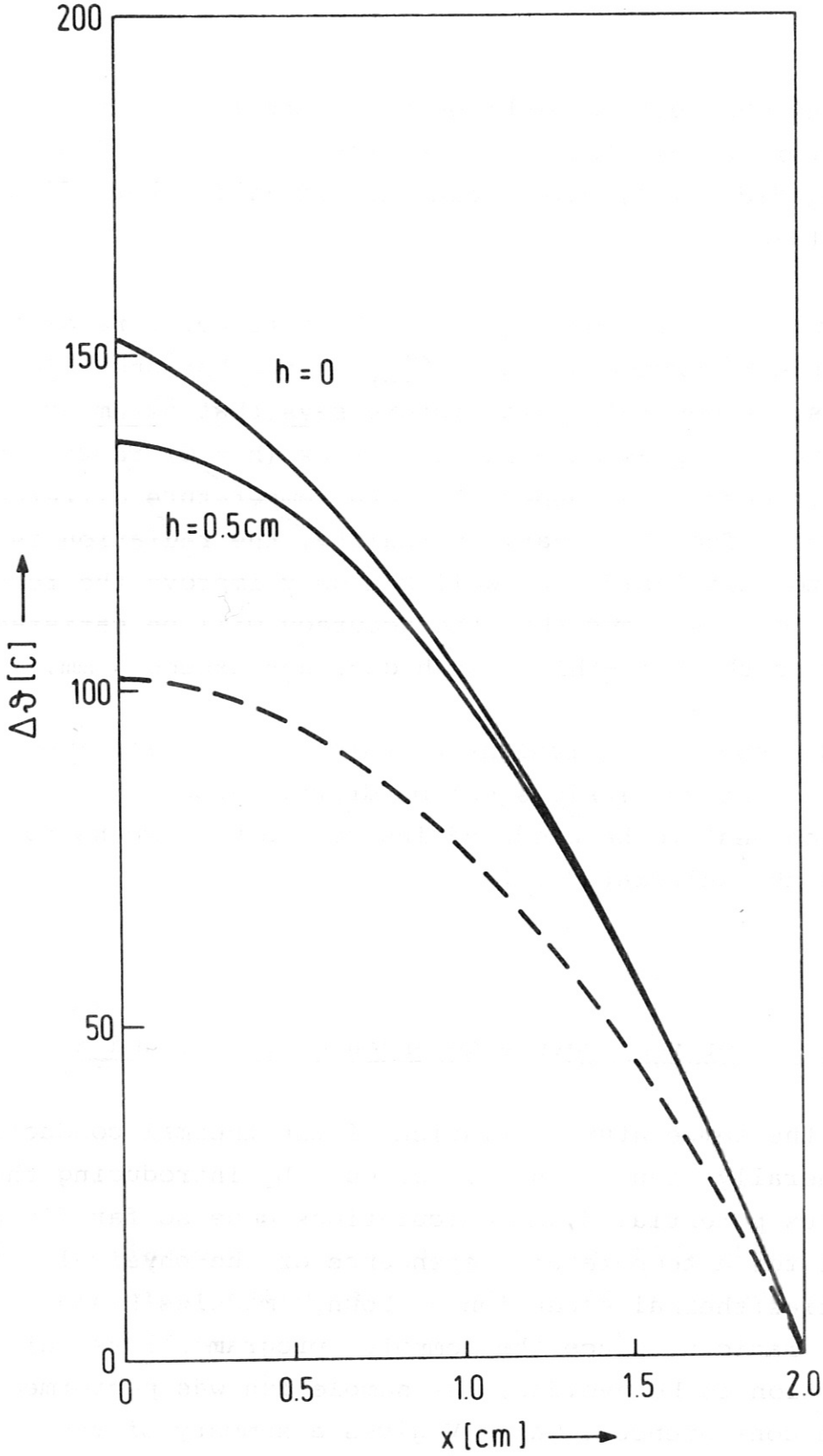

Fig. 16: Temperature profiles depending on the half thickness h of radiation absorption.

by asking what errors might occur if the radiation penetrates the wall for a characteristic length h instead of behaving "ideally", which means acting like a heat flux from outside.

The answer is given by fig. 17 for the temperature difference $\Delta\vartheta$ and the reference stresses σ_{ref} at the hot and cold surfaces. In general, this picture says that assuming all radiation acting as external heat flux (h = 0) represents the worst case with respect to both temperature difference and stress. The fact that, in reality, the radiation is converted to heat inside the wall can only improve the results. It additionally seems that the accuracy will be satisfactory as long as the half-thickness h does not exceed 1 mm.

Fig. 18 shows the equivalent picture for the lifetime. Here the same conclusions can be drawn. Assuming the radiation heat to be produced inside the wall means to prolong the calculated life.

4.3 Neglect of temperature dependence of E,ν, and α

Whilst the temperature variation of the thermal conductivity has generally been taken into account by introducing the heat flux potential S, all calculations done so far did not account for a temperature dependence of the physical properties: thermal expansion α, Young's modulus E and Poisson ratio ν. Since the computer program allows this restriction to be avoided, one sample run was performed to see the consequences. Table V gives a summary of the results.

It can be seen that neglecting the temperature dependence (IS2 = 0) leads to a slight increase in the reference stress at the hot surface. Since, for this special case, this surface is the critical one with respect to the lifetimes the

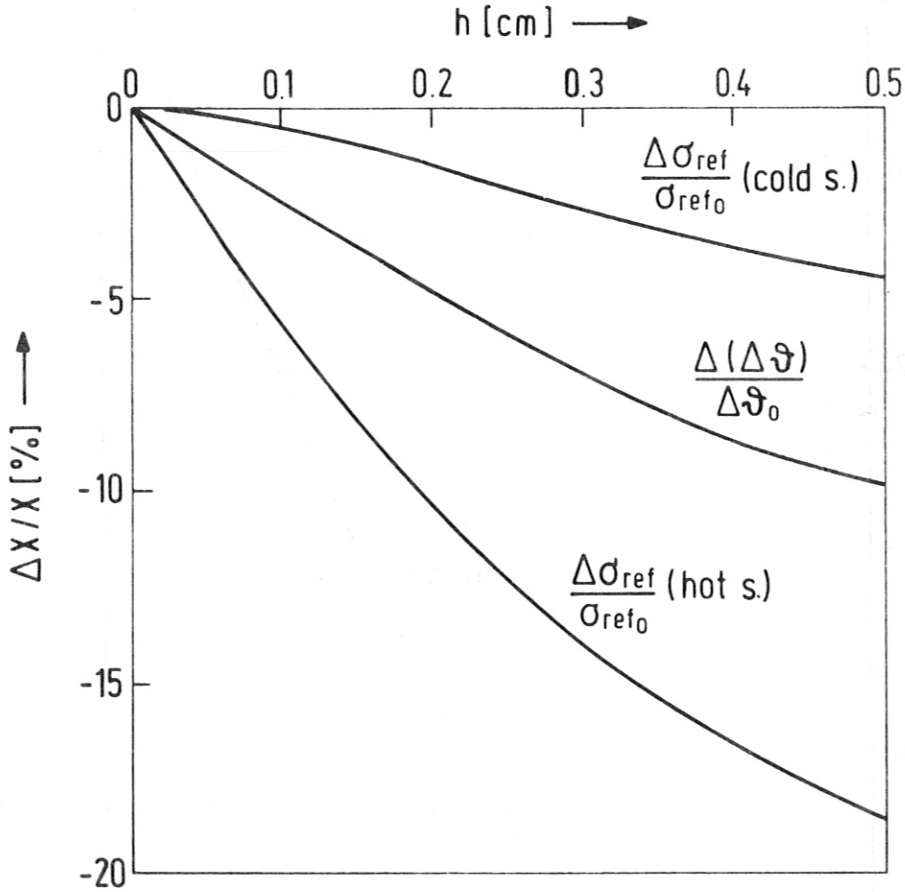

Fig. 17: Deviations in temperature differences and reference stresses at the hot and cold surfaces depending on the half thickness h of radiation absorption.

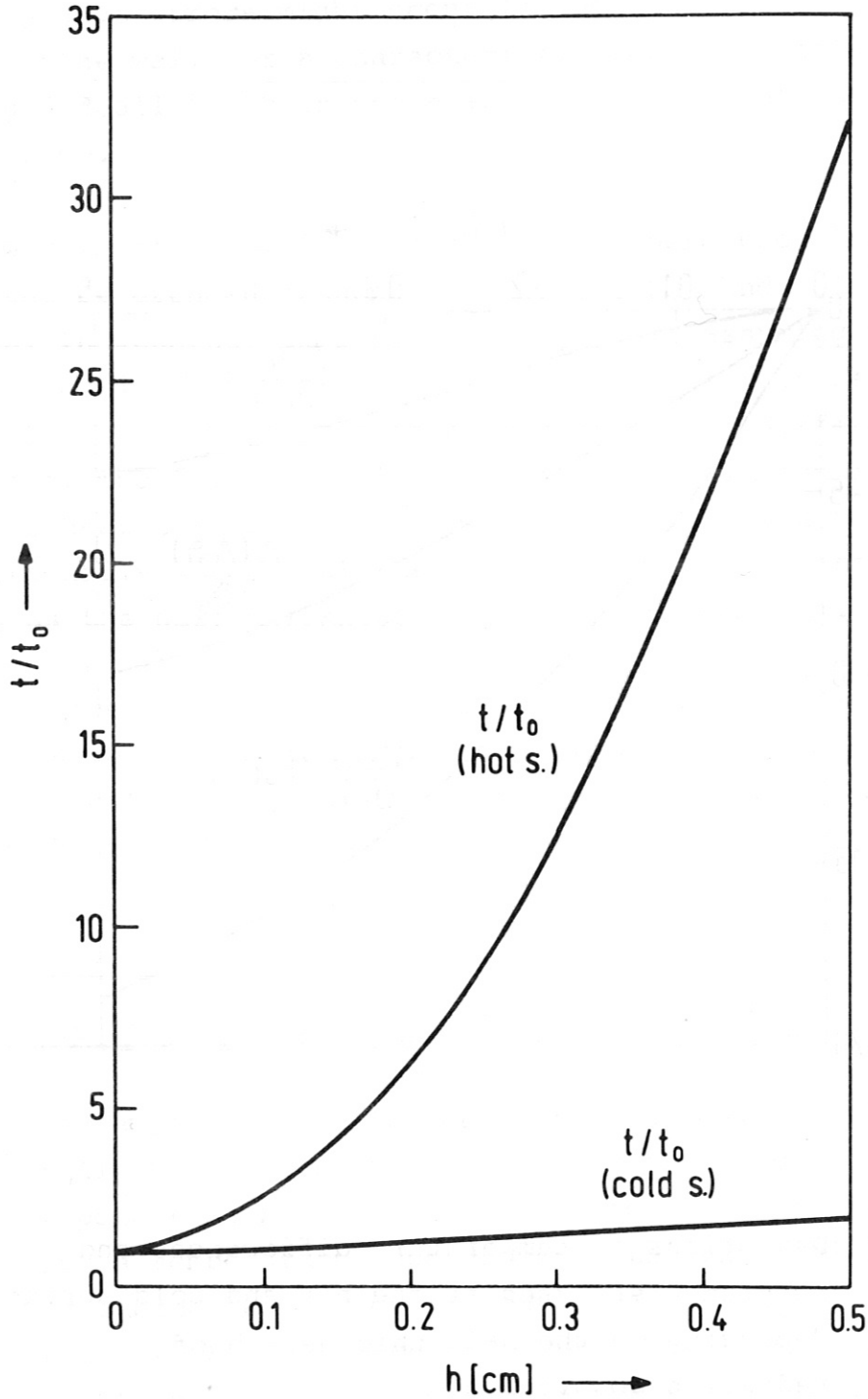

Fig. 18: Deviations in the calculated life t of the hot and cold surface depending on the half-value Thickness h of radiation absorption.

Table V: Results of calculations showing the influence of temperature dependence of E, ν, and α on the final results.

Assumptions:			
Neutron wall loading	PWN	= 100 W/cm^2	
Radiation wall loading	PWS	= 5 W/cm^2	
Half-thickness	HD	= 0.	
Wall thickness	TFW	= 2 cm	
Pressure load	PIN-PAU	= 0.	
Geometry	MOD	= -2 (spher.,convex)	
Radius of sphere	RA	= 30 cm	
Temperature dependence:		neglected	considered
Reference stress at hot surface	[kp/cm^2]	2066	2050
Reference stress at cold surface	[kp/cm^2]	3515	3655
Calculated life at hot surface	[h]	846	924
Calculated life at cold surface	[h]	325 800	180 400

neglect means staying on the safe side. This statement is underlined by the result for the lifetime calculated at this location. On the other hand,the stresses and lifetimes evaluated for the cold side of the wall are appreciably underestimated if the temperature dependence is neglected. As long as the critical surface does not change to the cool side this deviation does not matter. As will be shown in the next section, such a change can, in fact, occur.

4.4 Influence of pressure load

As was already outlined in section 4.1 and shown in fig. 13, the thermal stress distribution in a wall is such that compressive stresses occur at the hot surface, and tensile stresses at the cold surface. This is valid as long as the wall is assumed to be free of stress at the average wall temperature.

The fact that the hot surface is the most critical one with respect to the wall lifetime - at least in the cases presented so far - and that it is loaded by compressive stresses suggests an improvement of the mechanical performance if the wall element is loaded by an internal pressure. The results presented in table VI for a 2 cm thick wall prove this statement. A significant increase in the lifetime can be expected in the case where the stress level is dominated by thermal stresses.

If, however, the stress level is dominated by mechanical stresses,an increase of pressure worsens the situation and the calculated life decreases. This is to be expected in the case of thin walls,as is indicated by the results summarized in table VII for a 0.2 cm wall. Since in this case - with the exception of very low overpressures - the stresses of both the hot and the cold surface are tensile,even the critical surface can change to the cold side.

Table VI: Results of calculations showing the influence of an additional internal pressure; wall thickness t_{FW} = 2 cm .

Assumptions:			
Neutron wall loading	PWN	=	100 W/cm^2
Radiation wall loading	PWS	=	5 W/cm^2
Half-thickness	HD	=	0.
Wall thickness	TFW	=	2. cm
Pressure load	PIN-PAU	=	Δp (bar) varied
Geometry	MOD	=	-2 (spher., convex)
Radius of sphere	RA	=	30 cm

Δp	hot surface, 651.94 C				cold surface, 500.C			
[bar]	mech.stress*	therm.stress*	ref.stress*	life**	mech.stress*	therm.stress*	ref.stress*	life**
0.	0.	- 2066	2066	846	0	+ 3515	3517	325 800
10.	+ 67.	- 2066	1999	1242	+ 72	+ 3515	3597	229 900
2o.	+ 133	- 2066	1933	1845	+ 143	+ 3515	3678	163 600
30.	+ 200	- 2066	1866	2723	+ 215	+ 3515	3760	117 200
40.	+ 266	- 2066	1800	3990	+ 286	+ 3515	3842	84 620
50.	+ 333	- 3066	1733	5932	+ 358	+ 3515	3924	61 500

* stresses in [kp/cm^2]

** life in [h]

Table VII: Results of calculations showing the influence of an additional internal pressure; wall thickness t_{FW} = 0.2 cm.

Assumptions:	Neutron wall loading	PWN	= 100 W/cm^2
	Radiation wall loading	PWS	= 5 W/cm^2
	Half-thickness	HD	= 0.
	Wall thickness	TFW	= 0.2 cm
	Pressure load	PIN-PAU	= Δp (bar) varied
	Geometry	MOD	= -2 (spher., convex)
	Radius of sphere	RA	= 30 cm

Δp	hot surface, 506.13 C				cold surface, 500.C			
[bar]	mech.stress*	therm.stress*	ref.stress*	life**	mech.stress*	therm.stress*	ref.stress*	life**
0.	0	- 110	110	3.025(20)	0	+ 126	126	3.006(20)
10.	755	- 110	644	2.820(14)	+ 760	+ 126	896	2.325(13)
20.	1509	- 110	1399	7.344(10)	+ 1519	+ 126	1666	1.724(10)
30.	2264	- 110	2153	2.922(8)	+ 2279	+ 126	2436	9.612(7)
40.	3018	- 110	2908	3.306(6)	+ 3039	+ 126	3205	1.359(6)
50.	3773	- 110	3662	95710	+ 3798	+ 126	3975	50 500

* stresses in [kp/cm^2]

** life in [h]

4.5 Influence of geometry and restrain condition

Up to now the calculations reported have been exclusively for spherical geometry with convex curvature. In practice, this means that the reactor blanket may be constructed of a number of modules arranged along the minor and major circumferences, having spherical end cups which are directed radially towards the plasma. The outer radius of such a cup was assumed to be RA = 30 cm.

For comparison, we now assume the end cups to be cylindrical in one direction with a radius of RA = 30 cm; subsequently, we assume them to be plane circular plates of radius RA = 30 cm and, finally, to be square plates having side lengths of AA = BB = 30 cm. In all three cases we additionally vary the restrain condition, thus considering both perfect restrainment and free, axial or lateral expansion.

The results of these calculations are summarized in table VIII. It can be concluded from these figures that the cylindrical geometry yields similar results to the spherical geometry as long as thermal stresses dominate in the wall. The higher mechanical stresses in the cylindrical case are even advantageous with respect to the lifetime because they outweigh part of the thermal stresses. The fact whether the cylinder will be clamped or freely extendible does not matter very much.

As compared with these cases, the plane geometry calculations show the important influence of the mechanical stresses due to the internal pressure, which was assumed to be Δp = 30 bar. In the cases evaluated here none of the four possible solutions satisfies even the requirement of stresses to be below the short-time rupture strength. This means that only small overpressures can be applied in the case of plane first wall geometry using similar extensions.

Table VIII: Results of calculations showing the influence of geometry and restrain condition.

Assumptions:			
Neutron wall loading	PWN	=	100 W/cm^2
Radiation wall loading	PWS	=	5 W/cm^2
Half-thickness	HD	=	0.
Wall thickness	TFW	=	2 cm
Pressure load	PIN-PAU	=	30. bar
Geometry	MOD	=	varied
Add. extent	AA,BB,RA	=	30.

MOD	Restr. Cond.	temp.* difference	hot surface				cold surface			
			max.** mech.stress	therm.stress**	ref.stress**	life***	max.** mech.stress	therm.stress**	ref.stress**	life***
- 2	—	151.94	200	- 2066	1866	2723	215	3515	3760	117 200
- 1	restr.	147.97	414	- 2064	1813	5063	444	3382	3707	145 500
- 1	free	147.97	414	- 2064	1763	6793	444	3382	3744	125 300
0 circ.	restr.	144.14	3356	- 2062	1294	229 000	3356	3254	6609	—
0 circ.	free	144.14	8518	+ 602	9119	—	8518	591	9109	—
0 rect.	restr.	144.14	8810	- 2062	6431	—	8810	3254	10448	—
0 rect.	free	144.14	7847	+ 602	8448	—	7847	591	8438	—

* temperature differences in [^{o}C]

** stresses in [kp/cm^2]

*** life in [h]

5. CONCLUSIONS

The analysis of the mechanical behaviour of the first wall under steady-state load conditions and the computer program based on it which are both described in this report involve a minimum of ad hoc assumptions. Both the analysis and the computer program, however, permit the introduction of special simplifications which are usually made when considering this problem. Therefore,it is possible to study the influence of simplifying assumptions upon the final results - at least upon those results which are considered to be final in the scope of this analysis. These are essentially the temperature and stress load of the first wall.

A few simplifications have been investigated: the shape of the nuclear power density profile, the shape of the radiation power density profile, and the neglect of the temperature dependence of some physical material properties.

As far as the nuclear power density profile is concerned it has been shown that the assumption of a constant power density leads to an underestimation of the temperature and stress load. A linear approximation of the real profile, in contrast, yields rather accurate results with an accuracy of about + 0.5 %. This is valid at least for the power density profiles found in stainless steel walls.

The error introduced by assuming the plasma radiation to be an external heat flux to the wall instead of giving rise to internal heat sources cannot be explicitly assigned because the real penetration depth is dependent on the energy spectrum. If the radiation source is restricted to bremsstrahlung radiation alone, the error should not exceed 5 % in temperature and 10 % in stress load. For other radiation sources equivalent errors can be estimated if the energy is approximately known. In principle, the assumption of radiation to be an external source of heat - regardless of the radiation energy - puts the results on the safe side.

Taking into account the temperature dependence of material properties sometimes causes significant difficulties in the analysis. Therefore, average values are often applied. This is valid especially in the case of Young's modulus, Poisson ratio, and thermal expansion used in the course of stress analysis. From some few calculations it was found that such a simplifying assumption is justified in the case that the life of the wall is determined by the conditions at the hot surface. If, however, the conditions at the cold surface are the dominating ones an underestimation of stresses is the consequence.

Very often thermal stresses are estimated on the basis of a linear variation of temperature within the wall. This means, in practice, the neglect of any heat source inside the wall. The correct analysis described in this report shows that such an assumption is not justified. In fact, it puts the results on the safe side but it is believed that they are too far on the safe side as to permit conclusions close to reality. This is especially valid if the hot surface is the lifetime-limiting one. An overestimation of stresses by about a factor of 2 does not seem impossible.

Besides the intention of showing the influence of some simplifying assumptions, some first parameter studies just for orientation should be made. This was done by introducing a pressure load in addition to the thermal stresses and by considering the influence of the choice of geometry and restrain condition. It could be shown that an internal pressure in a module can have an advantageous effect in the sense that thermal stresses can be lowered. This holds especially in the case of thick walls. The reverse is valid for thin walls. As far as the geometry is concerned, it could be shown that plane wall elements can only be loaded by much smaller pressures than spherical or cylindrical elements of similar size. Though not surprising, these results give a first feeling for subsequent investigations.

REFERENCES

[1] B.Bädger et al.: UWMAK-I, A Wisconsin Toroidal Fusion Reactor Design; UWFDM-68 (1973)

[2] J.R. Stanbridge et al.: Design of Stainless Steel Blanket Cells for a Fusion Reactor; CLM-R127 (1974)

[3] W. Dänner: A Preliminary Model for Estimating the First Wall Lifetime of a Fusion Reactor; IPP 4/130 (1975)

[4] W. Dänner: Some Nuclear Characteristics of Liquid Lithium/Stainless Steel Fusion Reactor Blankets (to be published)

[5] S. Glasstone, R.H. Lovberg: Controlled Thermonuclear Reactions. Van Nostrand Reinhold Company, New York, Cincinnati, Toronto, London, Melbourne, 1960

[6] M. Barbier: Induced Radioactivity.North Holland Publ. Comp., Amsterdam, London 1969

[7] S. Timoshenko. J.N. Goodier: Theory of Elasticity, McGraw Hill Book Comp. Inc., New York. Toronto, London 1951

[8] W. Riezler, W. Walcher: Kerntechnik. B.G. Teubner Verlagsgesellschaft Stuttgart 1958

[9] R. Stephenson: Introduction to Nuclear Engineering. McGraw Hill Book Comp. Inc., New York, Toronto, London 1958

[10] Akad. Verein Hütte e.V., Berlin (ed.): Hütte, Des Ingenieurs Taschenbuch, Bd. I: Theoretische Grundlagen, 28. Aufl., Verlag von Wilhelm Ernst & Sohn, Berlin 1955

[11] S. Timoshenko, S. Woinowsky-Krieger: Theory of Plates and Shells. McGraw-Hill Book Company, Inc., New York, Toronto, London, 1959

[12] H. Neuber: Technische Mechanik. 2. Teil: Elastostatik und Festigkeitslehre. Springer-Verlag, Berlin, Heidelberg, New York 1971

[13] F.R. Larsen, J. Miller: A time-temperature relationship for rupture and creep stresses. Trans. ASME, July 1952, 765-775

[14] K.D. Clöß: Physikalische und mechanische Eigenschaften von Hüllmaterialien. PSB-Bericht Nr. 1001 (Phase IIa). KFZ Karlsruhe, 1968.

[15] K. Ehrlich: personal communication.